frontiers | Frontiers in Physiology

TYPE Original Research
PUBLISHED 09 October 2024
DOI 10.3389/fphys.2024.1434359

OPEN ACCESS

EDITED BY
Michael L Jennings,
University of Arkansas for Medical Sciences, United States

REVIEWED BY
Pawel Swietach,
University of Oxford, United Kingdom
Nazih Nakhoul,
School of Medicine, Tulane University, United States

*CORRESPONDENCE
Patrice G. Bouyer,
patrice.bouyer@valpo.edu
Walter F. Boron,
Walter.Boron@case.edu

RECEIVED 17 May 2024
ACCEPTED 28 August 2024
PUBLISHED 09 October 2024

CITATION
Bouyer PG, Salameh AI, Zhou Y, Kolba TN and Boron WF (2024) Effects of extracellular metabolic acidosis and out-of-equilibrium CO_2/HCO_3^- solutions on intracellular pH in cultured rat hippocampal neurons. *Front. Physiol.* 15:1434359. doi: 10.3389/fphys.2024.1434359

Effects of extracellular metabolic acidosis and out-of-equilibrium CO_2/HCO_3^- solutions on intracellular pH in cultured rat hippocampal neurons

Patrice G. Bouyer[1,2]*, Ahlam I. Salameh[3,4], Yuehan Zhou[1,4], Tiffany N. Kolba[5] and Walter F. Boron[1,4]*

[1]Department of Cellular and Molecular Physiology, Yale University School of Medicine, New Haven, CT, United States, [2]Department of Biology, Valparaiso University, Valparaiso, IN, United States, [3]Preclinical Sciences Division, Kent State University College of Podiatric Medicine, Independence, OH, United States, [4]Department of Physiology & Biophysics Case Western Reserve University School of Medicine, Cleveland, OH, United States, [5]Department of Mathematics & Statistics, Valparaiso University, Valparaiso, IN, United States

Metabolic acidosis (MAc)—an extracellular pH (pH_o) decrease caused by a $[HCO_3^-]_o$ decrease at constant $[CO_2]_o$—usually causes intracellular pH (pH_i) to fall. Here we determine the extent to which the pH_i decrease depends on the pH_o decrease vs the concomitant $[HCO_3^-]_o$ decrease. We use rapid-mixing to generate out-of-equilibrium CO_2/HCO_3^- solutions in which we stabilize $[CO_2]_o$ and $[HCO_3^-]_o$ while decreasing pH_o (pure acidosis, pAc), or stabilize $[CO_2]_o$ and pH_o while decreasing $[HCO_3^-]_o$ (pure metabolic/down, pMet↓). Using the fluorescent dye 2′,7′-bis-2-carboxyethyl)-5(and-6)carboxyfluorescein (BCECF) to monitor pH_i in rat hippocampal neurons in primary culture, we find that—in naïve neurons—the pH_i decrease caused by MAc is virtually the sum of those caused by pAc (~70%) + pMet↓ (~30%). However, if we impose a first challenge (MAc_1, pAc_1, or $pMet↓_1$), allow the neurons to recover, and then impose a second challenge (MAc_2, pAc_2, or $pMet↓_2$), we find that pAc/pMet↓ additivity breaks down. In a twin-challenge protocol in which challenge #2 is MAc, the pH_o and $[HCO_3^-]_o$ decreases during challenge #1 must be coincident in order to mimic the effects of MAc_1 on MAc_2. Conversely, if challenge #1 is MAc, then the pH_o and $[HCO_3^-]_o$ decreases during challenge #2 must be coincident in order for MAc_1 to produce its physiological effects during the challenge #2 period. We conclude that the history of challenge #1 (MAc_1, pAc_1, or $pMet↓_1$)—presumably as detected by one or more acid-base sensors—has a major impact on the pH_i response during challenge #2 (MAc_2, pAc_2, or $pMet↓_2$).

KEYWORDS

CO_2/HCO_3^- out of equilibrium solutions, pH regulation, HCO_3^- sensor pH_o sensor, acid base, neuron

Introduction

Neuronal activity produces transient shifts in extracellular pH (pH_o). The direction of these shifts depends on the location in the brain, and their peak magnitude depends on the intensity and duration of the activity (for review, see Chesler, 2003). Conversely, changes in pH_o can alter neuronal excitability by modulating pH-sensitive ion channels (Meech and Thomas, 1987; Tang et al., 1990; Church et al., 1998). Moreover, changes in pH_o also cause intracellular pH (pH_i) to shift in the same direction (Ellis and Thomas, 1976; Vaughan-Jones, 1986; Tolkovsky and Richards, 1987; Bouyer et al., 2004) and such changes in pH_i also modulate neuronal excitability (Filosa et al., 2002; Wang et al., 2002). In addition to these effects on ion channels, changes in pH_o and/or pH_i can modulate other components of the machinery of neurotransmission, such as vesicular amine transporters, and transporters that mediate the reuptake of glutamate and serotonin (Keyes and Rudnick, 1982; Kanai et al., 1995; Eiden et al., 2004). Therefore, it is important for a neuron to maintain an appropriate pH_i in the face of shifting values of pH_o. To achieve this task, neurons like other cells, are armed with acid-base transporters (Ruffin et al., 2014). Among these, Na-H exchangers play important roles in maintaining steady-state pH_i as well as in extruding acid during the recovery of pH_i from an acid-load (Bevensee et al., 1996; Raley-Susman et al., 1991; Tolkovsky and Richards, 1987; Yao et al., 1999). In neurons exposed to CO_2/HCO_3^-, the Na^+-coupled HCO_3^- transporters—the Na^+-driven Cl/HCO_3 exchanger (Boron and De Weer, 1976; Russell and Boron, 1976; Thomas, 1977) and the electroneutral Na/HCO_3 cotransporters NBCn1 and NBCn2 (Cooper et al., 2005; Parker et al., 2008)—are among the most potent acid extruders (i.e., transporters that mediate the efflux of H^+ or influx of alkali; see refs. Schwiening and Boron, 1994; Cooper et al., 2005; 2009; Gurnett et al., 2008). In the presence of CO_2/HCO_3^-, the $Cl\text{-}HCO_3$ exchanger AE3 is a potent acid loader that helps neurons to recover after alkaline loads (Kopito et al., 1989; Raley-Susman et al., 1993; Brett et al., 2002; Hentschke et al., 2006; Svichar et al., 2009; Ruffin et al., 2014; Salameh et al., 2017).

Although the field has witnessed substantial progress in clarifying the molecular nature of the Na-H exchangers (Donowitz et al., 2013) and HCO_3^- transporters (Parker and Boron, 2013; Romero et al., 2013; Thornell et al., 2025) that are involved in pH_i homeostasis, the same is not true for understanding how changes in the key extracellular acid-base parameters—pH_o, $[CO_2]_o$, and $[HCO_3^-]_o$—modulate these transporters and, thus, pH_i. Of course, changes in the above parameters could directly affect transporters. For example, a change in pH_o would modulate Na-H exchange because H^+ competes with extracellular Na^+ (Aronson et al., 1982). Change in pH_o or $[HCO_3^-]_o$ would modulate the Na^+-coupled HCO_3^- transporters because in at least two cases, and possibly all, the HCO_3^--related substrate is $CO_3^=$ or $NaCO_3^-$ (Lee et al., 2023), the concentrations of which are very sensitive to changes in pH_o and $[HCO_3^-]_o$. One mechanism by which metabolic acidosis (MAc; a decrease in $[HCO_3^-]_o$ that causes pH to fall) causes pH_i in neurons to fall (Bouyer et al., 2004; Salameh et al., 2014) is an enhanced activity of an acid loader, the $Cl\text{-}HCO_3$ exchanger AE3 (Salameh et al., 2017).

One mechanism for the aforementioned enhanced AE3 activity is the fall in $[HCO_3^-]_o$ that accompanies MAc. However, other potential mechanisms could involve sensors for pH, CO_2, or HCO_3^- (Tresguerres et al., 2010) that respond to changes in acid-base status by modulating acid-base transporters. Established acid-base sensors include three G-protein–coupled proteins—GPR68 (aka, OGR1; see (Ludwig et al., 2003; Tomura et al., 2005; Mohebbi et al., 2012), GPR4 (Ludwig et al., 2003; Sun et al., 2010), and GPR65 (aka, TDAG8; see Ishii et al., 2005)—that activate in response to decreases in pH_o. In addition, the soluble adenylyl cyclase sAC (Chen et al., 2000) and certain receptor guanylyl cyclases (Schulz et al., 1998; Sun et al., 2009) become more active in response to increases in $[HCO_3^-]_i$; numerous ion channels (e.g., TASK, ASIC, TRPV) respond to changes in pH_o or pH_i (for reviews, see Montell, 2001; Lesage, 2003*a*; Holzer, 2009; Tresguerres et al., 2010); and the tyrosine kinase Pyk2 becomes more active in response to decreases in pH_i (Li et al., 2004). In *Drosophila*, Gr21a and Gr63a are reported to be CO_2 receptors; ectopic expression of Gr21a and Gr63a confers chemosensitivity to olfactory neurons, whereas gene deletion prevents behavioral response of *Drosophila* to CO_2 (Jones et al., 2007). Finally, the receptor protein tyrosine phosphatase γ (RPTPγ) appears to respond oppositely to changes in both $[CO_2]_o$ and $[HCO_3^-]_o$ but is insensitive to pH_o changes (Boedtkjer et al., 2016; Zhou et al., 2016). The review by Thornell et al. (2024) discusses such acid-base sensors.

The development of out-of-equilibrium (OOE) CO_2/HCO_3^- solutions (Zhao et al., 1995)—which can have virtually any combination of $[CO_2]$, $[HCO_3^-]$, and pH in the pathophysiological range of pH values—makes it possible to ask whether cells have a mechanism for sensing extracellular CO_2 or HCO_3^- *per se*, independent of pH. Indeed, using OOE solutions, Zhou et al. demonstrated that isolated renal proximal tubules increase their rate of bicarbonate reabsorption (i.e., H^+ secretion) in response to isolated decreases in basolateral $[HCO_3^-]$ (i.e., holding basolateral $[CO_2]$ and pH constant) or to isolated increases of basolateral $[CO_2]$, but not to isolated changes in basolateral pH_o (Zhou et al., 2005). These results were the first to demonstrate unequivocally that, independent of pH, the two components of the major blood buffer—CO_2/HCO_3^-—can act as potent modulators of a biological function.

An earlier study of cultured rat neurons showed that the pH_i responses to extracellular respiratory acidosis (i.e., an increase in $[CO_2]_o$ that causes pH_o to fall), to extracellular respiratory alkalosis (i.e., a decrease in $[CO_2]_o$), or to metabolic alkalosis (i.e., an increase in $[HCO_3^-]_o$, at fixed $[CO_2]_o$, that causes pH_o to rise) were each indistinguishable between medullary-raphé (MR) vs hippocampal (HC) neurons. In all cases, neuronal pH_i changed in the same direction as pH_o, with a steady-state $\Delta pH_i/\Delta pH_o$ of ~60%. However, the responses to extracellular metabolic acidosis were not uniform. The majority of the MR neurons and the minority of HC neurons exhibited the expected response to MAc: a reversible pH_i decrease and a $\Delta pH_i/\Delta pH_o$ of ~65%. In contrast to these "MAc-sensitive" neurons, a minority subpopulation of MR neurons and the majority of HC neurons exhibited a $\Delta pH_i/\Delta pH_o$ of only ~9% (Bouyer et al., 2004). Moreover, returning these "MAc-resistant" neurons from the MAc solution to a solution with a normal acid-base status causes pH_i to rebound above the initial baseline. An analysis of various possibilities (see the discussion of Bouyer et al., 2004), led to the hypothesis that MAc-resistant MR and HC neurons have an extracellular "HCO_3^- sensor" that can detect decreases in

TABLE 1 Physiological solutions.

	1	2	3	4	5			6		
	Standard CO_2/HCO_3^- -free	Standard CO_2/HCO_3^-	MAc	Ac (no CO_2/HCO_3^-)	pAc (OOE)			pMet↓ (OOE)		
Components					A	B	Mixture	A	B	Mixture
NaCl	128	102	110	128	97	105	101	113	105	109
NaH_2PO_4	1.3	1.3	1.3	1.3	2.6		1.3		2.6	1.3
$NaHCO_3$	0	22	14	0	44		22	28		14
KCl	3	3	3	3	6		3	6		3
$MgCl_2$	2	2	2	2		4	2	4		2
$CaCl_2$	2	2	2	2		4	2	4		2
Glucose	10	10	10	10		20	10		20	10
CO_2 (%)	0	5	5	0	10	0	5	10	0	5
HEPES	32.5	32.5	32.5	32.5		65	32.5		65	32.5
pH					7.40	7.18		7.20	7.43	
Final pH	7.40	7.40	7.20	7.20			pH 7.20			pH 7.40

The concentrations are in mM, except for CO_2 given in %. All solutions were titrated to the indicated pH at 37°C and osmolarities were adjusted to 300 ± 003 mOsm. The two out-of-equilibrium (OOE) were generated by rapid mixing as previously described (Zhao et al., 1995; 2003). Note that all nominally CO_2-free solutions were vigorously gassed with 100% O_2.

$[HCO_3^-]_o$ *per se*, and respond with a near-instantaneous increase in the rate of acid extrusion over acid loading, the effect of which is to minimize decreases in pH_i.

In the present study, we re-examine the effect of MAc on the pH_i of rat HC neurons by using OOE technology to break MAc artificially into its two component parts, "pure" acidosis (pAc: ↓pH_o at fixed $[CO_2]_o$ and $[HCO_3^-]_o$) and pure metabolic/down (pMet↓: ↓$[HCO_3^-]_o$ at fixed $[CO_2]_o$ and pH_o). We also examined acidosis (Ac) in the nominal absence of CO_2/HCO_3^-. Finally, we performed seven twin-challenge protocols in which we examined the effect on pH_i of a challenge (e.g., pMet↓), followed by a recovery period, and then a second challenge (e.g., MAc). Surprisingly, we find that the effects of pAc and pMet↓ do not necessarily sum, and that neurons often respond to pMet↓ by with a paradoxical pH_i increase.

Methods

Cell culture

We performed experiments on rat cultured hippocampal neurons, with approval for all animal procedures from the Yale University Animal Care and Use Committee. The methods to culture neurons are essentially the same as previously described (Brewer et al., 1993) and subsequently modified in the Boron laboratory (Chen et al., 2008). Briefly, a pregnant rat was deeply anesthetized using halothane, prior to cervical dislocation. Rat embryos (18 days) were quickly removed from the uterus and decapitated. Approximately ten brains were collected and placed in filtered HEPES-buffered solution (HBS) containing (in mM): NaCl, 143.7; KCl, 3; and HEPES, 10. Hippocampi were extracted using fine forceps and a scalpel and then exposed to 0.03% (w/v) trypsin (Sigma-Aldrich, St Louis, MO) dissolved in HBS for 15 min at 37°C. Using flamed Pasteur pipettes with reduced tip diameter, we triturated the tissues to disperse cells. Neurons were plated in neurobasal medium supplemented with B-27 (GIBCO-Invitrogen, Carlsbad, CA), 10% fetal calf serum (FCS), plus penicillin-streptomycin on poly-L-lysine (MP Biomedical, Irvine, CA) coated glass coverslips (Warner Instruments, Hamden CT, USA) or photoetched grid coverslips (Bellco Biotechnology, Vineland, NJ). After 3–4 h the medium was changed to a similar one without FCS. Neurons cultures were kept in a 5% CO_2-air incubator at 37°C for at least seven and up to 61 days (average 23 days).

Solutions

Table 1 lists the compositions of the physiological solutions, which were adjusted to 300 ± 3 mosmoles/kg using a vapor pressure osmometer (Model 5520C, Wescor, Inc., Logan UT). All solutions were delivered by syringe pumps (model #55-2222, Harvard Apparatus, South Holliston, MA, USA) at 7 mL min^{-1} through Tygon tubing that connected to a water-jacket system for warming before being delivered to a chamber (Bouyer et al., 2003). The temperature in the chamber was 37°C.

To generate CO_2/HCO_3^- out-of-equilibrium solutions, we followed the procedures originally described by the Boron laboratory (Zhao et al., 1995; 2003; Zhou et al., 2005), and we adapted them for hippocampal neuron solutions. For a review, see (Boron, 2004). In addition, the accompanying *Hypothesis and Theory* contribution contains a figure and an examples of how we implemented the OOE approach in the present study (Bouyer et al., 2024). Briefly the contents of two syringes (having the composition A and B in Table 1) were rapidly mixed at T connector connected to short Tygon tubing containing nylon

mesh to promote mixing. The short length of Tygon tubing filled with mesh was connected to a chamber with a channel 2.5 mm wide × 14 mm long to promote laminar flow.

Fluorescence measurements

We followed the same protocol previously described for fluorescence measurements in cultured neurons (Bouyer et al., 2004). Neurons were loaded with the pH-sensitive dye 2′,7′-bis-2-carboxyethyl)-5(and-6) carboxyfluorescein (BCECF) by incubating cells at room temperature for ~15 min in solution 1 (Table 1) containing 10 μM of the esterified BCECF (Molecular Probes Inc., Eugene, OR). Fluorescence measurements started ~5 min after we began to flow solution one or 2 (Table 1) through the chamber to warm cells and flush unhydrolyzed BCECF.

We used an Olympus IX70 inverted microscope equipped for epi-fluorescence (oil immersion ×40 objective, NA 1.35, with a ×1.5 magnification knob) to locate neurons on the field. The light was generated by 75-W xenon arc lamp and the two excitations wavelength of 440 nm and 490 nm were obtained by two excitations filters (440 ± 5 nm and 495 ± 5 nm, Omega Optical Inc., Brattleboro, VT) mounted on a filter wheel (Ludl Electronic Products Ltd., Hawthorne, NY) in the excitation light path. Selected neutral density filters (Omega Optical, Inc.), mounted on a second wheel, were used to equalize as nearly as possible the emitted light and avoid over-illumination of the cells. The excitation light was directed to the cells via a long-pass dichroic mirror (DM 510, Omega Optical Inc.), and we collected the emission light via a band-pass filter (530 ± 35 nm, Omega Optical Inc.) connected to intensified CCD camera (Model 350F, Video Scope International LTD, Dulles, VA). We averaged signals from 4 video frames at an acquisition rate of ranging from once every 2.5–20 s; a shutter on the filter wheel protected the cells and filters from the light between acquisitions. The data acquisition was controlled by software developed in our laboratory using the Optimas (Media Cybernetics, Inc., Silver Spring, MD) platform. Using Optimas, we delineated an area of interest (AOI) corresponded mostly to the soma of the cell and the pixel intensity of the AOI at 490 (I_{490}) was divided by the pixel intensity at 440 (I_{440}) nm. The fluorescence ratio I_{490}/I_{440} was converted to pH_i values by using the high-K^+/nigericin technique (Thomas et al., 1979), as modified in the Boron laboratory to obtain a one-point calibration at pH_i 7.00 (Boyarsky et al., 1988).

We generated, in a separate set of experiments, the calibration curve for BCECF, by flowing through the chamber 10 different solutions with pH values ranging from 5.8 to 8.5 to generate the parameters for the aforementioned one-point calibration. The best fit value pK was 7.13 ± 0.005 (SD), and the *b* value (i.e., the difference between R_{max} and R_{min}) was 1.97 ± 0.009 (SD). High-K^+/nigericin solutions were delivered to the chamber though a system independent of that used to superfuse the cells to avoid nigericin contamination in the lines during the actual experiments (Richmond and Vaughan-Jones, 1997; Bevensee et al., 1999). At the end of each experiment, we washed extensively the chamber with 70% ethanol and deionized water.

Definitions

State

Our definitions of the states of MAc "resistance" vs MAc "sensitivity" follow the criteria adopted by Salameh et al. (2014). State applies to the size of a single pH_i change (ΔpH_i) during a single acid-base challenge. In a twin-pulse protocol, each challenge has its own state. For each challenge, a neuron is resistant when $(\Delta pH_i/\Delta pH_o) \leq 40\%$, where ΔpH_i is the change in pH_i caused by ΔpH_o, the imposed change in pH_o. Conversely a neuron is sensitive when $(\Delta pH_i/\Delta pH_o)$ is larger than 40%. Although figure 40% is somewhat arbitrary, it coincides with a natural break in the data of Salameh et al. (2014). In the twin-pulse protocols in Figure 3B through Figure 9B in Results, we use the subscript "1" to refer to the first of the two challenges, and the subscript "2" to refer to the second. In these seven figures, we plot $(\Delta pH_i)_1$ for each neuron on the *x*-axis, and the corresponding $(\Delta pH_i)_2$ on the *y*-axis. We indicate the resistant-sensitive boundaries by dashed blue lines, vertical for $(\Delta pH_i)_1$ and horizontal for $(\Delta pH_i)_2$.

"State" is defined by the location of the cell on the $[(\Delta pH_i)_1,(\Delta pH_i)_2]$ coordinate system, with respect to the dashed blue lines. Thus, if a neuron is to the left of the vertical dashed blue line, the state is MAc_1 sensitive; if below the horizontal dashed blue line, the state is MAc_2 sensitive. If the neuron lies on the opposite side of either line, the state is resistant. The intersecting dashed blue lines define four "quadrants" that we will discuss, with examples, in conjunction with Figure 3B.

Behavior

Our definitions of the behaviors of "adaptation" vs "consistency" vs "decompensation" also follow the criteria adopted by Salameh et al. (2014). "Behavior" has meaning only during a twin-pulse protocol in which a cell (1) is subjected to acid-base challenge #1, (2) is allowed to recover, and (3) is subjected to acid-base challenge #2. The pH_i changes during the two challenges are $(\Delta pH_i)_1$ and $(\Delta pH_i)_2$. The determination of behavior revolves around the hourglass analysis (see B panels in Figure 3 through Figure 9) In brief, the dashed gray line that slopes upward from lower left to upper right at 45° represents identity, that is, $(\Delta pH_i)_1 = (\Delta pH_i)_2$. The sets of solid gray curves shaped like a tilted hour glass indicate our upper and lower confidence limits, based on (1) a requirement that $(\Delta pH_i)_2$ be $(10^{0.05}–1)$, which is ~12.2%, greater than $(\Delta pH_i)_1$ in the case of the upper asymptote of the hourglass or $(10^{0.05}–1)$ less than $(\Delta pH_i)_1$ in the case of the lower asymptote, and (2) an assumed experimental uncertainty of ±0.02 pH units. Thus,

$$Upper\ asymptote:\ (\Delta pH_i)_2 = (\Delta pH_i)_1 + \left(\left[10^{(+0.05)}\right] - 1\right) \cdot \left|(\Delta pH_i)_1\right| + 0.02 \quad (1)$$

$$Lower\ asymptote:\ (\Delta pH_i)_2 = (\Delta pH_i)_1 - \left(\left[10^{(+0.05)}\right] - 1\right) \cdot \left|(\Delta pH_i)_1\right| - 0.02 \quad (2)$$

where $|(\Delta pH_i)_1|$ indicates the absolute value.

"Behavior" is defined by the location of the cell on the $[(\Delta pH_i)_1, (\Delta pH_i)_2]$ coordinate system, with respect to the upper and lower

asymptotes. Thus, if $(\Delta pH_i)_2$ lies above the upper asymptote of the hourglass—that is, when $(\Delta pH_i)_2$ is sufficiently > $(\Delta pH_i)_1$—Salameh et al. (2014) defines the neuron as showing adaptation. If $(\Delta pH_i)_2$ lies within the limits of the hourglass)—that is, $(\Delta pH_i)_2 \cong (\Delta pH_i)_1$—Salameh et al. defines the neuron as showing consistency. Finally, if $(\Delta pH_i)_2$ lies below the lower asymptote of the hourglass—that is, when $(\Delta pH_i)_2$ is sufficiently < $(\Delta pH_i)_1$—Salameh et al. defines the neuron as showing decompensation. We will provide examples in conjunction with Figure 3B.

Data analysis and statistics

For each pH_i experiment, we computed the fractional rate of the BCECF dye loss ($-k_{440}$) to assess cell viability with time (Bevensee et al., 1995). We choose to reject experiments with a rate–k_{440} > 5%.mn^{-1}. Data are reported as mean ± SD, followed by the number of cells (n), the number of coverslips (N), and the number of cultures ($\mathcal{N}$). Data were obtained from at least three different batches (i.e., obtained from at least three different litters of pups) of cultured cells. The SD values were computed on the basis of n. Means were compared using, as indicated, paired and unpaired Student's *t-tests* (two tails), using Microsoft Excel Analysis ToolPak or Kaleidagraph (Synergy Software, Perkiomen PA, USA). Proportions were compared using z-tests; $p < 0.05$ was considered significant. Curve fitting was performed using Kaleidagraph. Correlation strength for linear fits was assessed by R^2 values, and we considered a correlation to be weak when $R^2 < 0.2$; mild, for 0.2–0.4; moderate, 0.4–0.6; moderately strong for 0.6–0.8; and "strong linear relationship" for 08–1.0, as previously described (Vittinghoff et al., 2005; cited in Salameh et al., 2014). Linear mixed-effects models were used to incorporate the culture date as a random effect, with likelihood ratio tests used to ascertain the significance of the culture date, using the lmerTest package in R (R version 4.4.1, https://www.r-project.org/).

Results

Ability of metabolic acidosis to change pH_i

In a previous study (Bouyer et al., 2004), we found that exposing cultured rat hippocampal neurons (a total of 14) to a single challenge of metabolic acidosis caused relatively little fall in pH_i in the majority of HC neurons, and a larger acidification in a minority of HC neurons. In the present study, we subject a much larger number of HC neurons to extracellular MAc (5% CO_2/14 mM HCO_3^-, pH = 7.20; solution 3, Table 1). Moreover, we now impose two sequential acid-base challenges per cell, and exploit out-of-equilibrium solutions to tease apart the contributions of a decreased pH_o *per se* and a decreased $[HCO_3^-]_o$ *per se*. For HC neurons in which we present MAc as the first acid-base challenge, we find that the average MAc-induced pH_i change (measured at times that we judged pH_i to be approximately stable) is −0.11 ± 0.10 (n = 235 cells, N = 86 coverslips, $\mathcal{N}$ = 35 cultures), where the negative sign denotes a pH_i decrease.

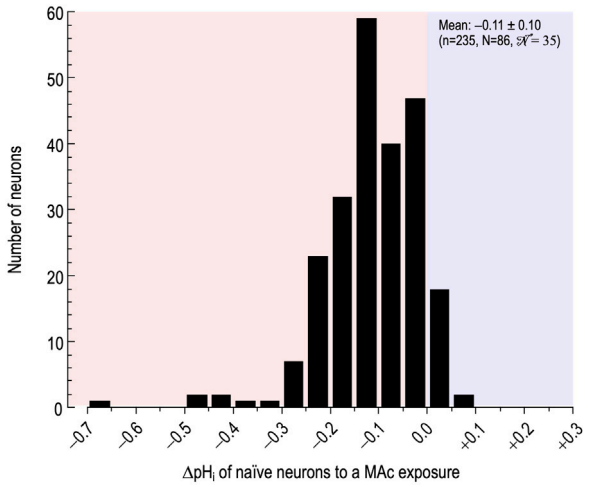

FIGURE 1
Effect of metabolic acidosis (MAc) on the pH_i of naïve rat hippocampal neurons. The histogram represents the distribution of the change in pHi (ΔpH_i)—judged after a time in MAc when we judged pH_i to be approximately stable—of neurons, caused by switching the extracellular solution from standard CO_2/HCO_3^- (solution 2, Table 1) to MAc (solution 3, Table 1). Here, we restrict the analysis to naïve neurons, that is, those for which MAc was the first challenge. The bin width is 0.05 pH units. n, number of neurons; N number of cover slips; $\mathcal{N}$, number of cultures. The MAc-induced ΔpH_i was 0.11 ± 0.10 (mean ± SD).

Figure 1 summarizes the distribution of pH_i changes (ΔpH_i). Using the definitions of MAc-resistant and MAc-sensitive cells (see Definitions[1]) and previously established (Salameh et al., 2014) we find that 90 neurons (~38%) were MAc-resistant and 145, MAc-sensitive (~62%). These percentages are nearly identical to those from a study on cultured mouse HC neurons (Salameh et al., 2014). We will refer to MAc-resistant vs MAc-sensitive as physiological "states."

Note that, although the vast majority of neurons respond to MAc with the expected acidification (i.e., negative ΔpH_i values in Figure 1, reddish background), in few cells, MAc paradoxically elicits an alkalinization (i.e., positive ΔpH_i values at the extreme right of Figure 1, blueish background).

Relationships between MAc-induced ΔpH_i and time in culture, and initial steady state pH_i

Time in culture and ΔpH_i during MAc

To determine whether the pH_i response to MAc depends on time in culture, in Figure 2A we plot the ΔpH_i of naïve neurons as a function of time, and find no correlation (R^2 = 0.002).

1 See Methods > Definitions.

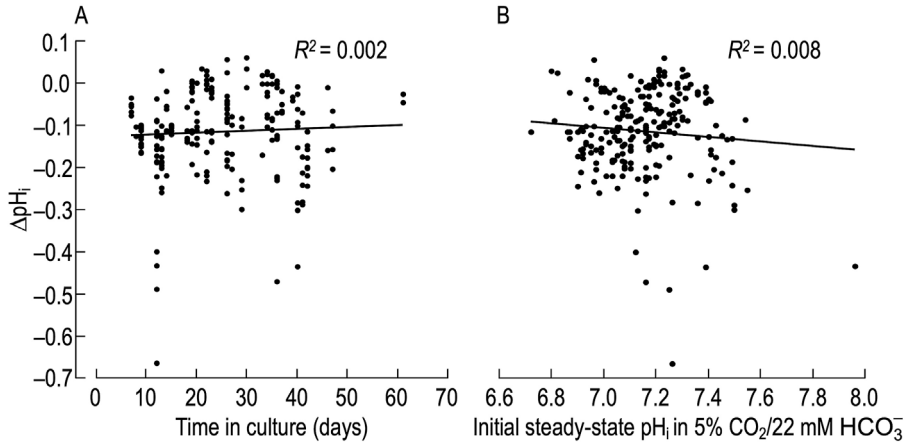

FIGURE 2
Relationship between pH_i change induced by metabolic acidosis (MAc) in naïve rat hippocampal neurons *versus* time in culture and initial steady-state pHi **(A)**, change in pH_i (ΔpH_i)—judged after a time in MAc when we judged pH_i to be approximately stable—vs. time in culture. We induced the ΔpH_i by switching the extracellular solution from standard CO_2/HCO_3^- (solution 2, Table 1) to MAc (solution 3, Table 1). As in Figure 1, we restrict the analysis to naïve neurons, that is, those for which MAc was the first challenge. The linear fit regression fit shows no correlation between ΔpH_i vs time in culture. **(B)**, change in pH_i vs initial steady-state pH_i value. These are the same ΔpH_i data as in panel **(A)**. The linear regression fit shows no correlation between ΔpH_i and pH_i values.

Impact of culture date on ΔpH_i

We maintained uniform conditions for each of the seven twin-challenge protocols that we present in the remainder of Results: MAc-MAc, Ac-MAc, MAc-Ac, pAc-MAc, MAc-pAC, pMet↓-MAc and MAc-pMet↓. Thus, we should not expect to observe systematic differences in ΔpH_i according to the culture date. To examine that possibility, we used a linear mixed-effects model to determine if culture date represents a significant predicator of the relationship between the pH_i just before the first of two challenges and the ΔpH_i during that challenge. Of the seven protocols, the random effect of culture date was significant only for two, MAc-MAc ($\chi^2(1) = 15.8$, $p < 0.001$) and pAc-MAc ($\chi^2(1) = 28.2$, $p < 0.001$). The most likely explanation is that these two instances of significance reflect random fluctuations, rather than biological effects, inasmuch as experimental conditions were uniform for each of the seven protocols.

Correlation between initial pH_i and ΔpH_i

We know from work of the Boron and the Church laboratories on HC neurons that, upon switching from a HEPES-buffered to a CO_2/HCO_3^--buffered extracellular solution, the initial steady-state pH_i impacts the direction (i.e., acidification vs alkalinization) and magnitude of the ensuing pH_i response (Schwiening and Boron, 1994; Bevensee et al., 1996; Smith et al., 1998). To test the hypothesis that the initial steady-state pH_i in CO_2/HCO_3^- may also influence the degree of MAc-induced acidification, in Figure 2B we plot the ΔpH_i of naïve neurons vs the initial pH_i, and find no correlation between the two parameters (R^2 = 0.008). Therefore, we conclude that factors other than time in culture and initial steady-state pH_i are responsible for the different pH_i responses observed during an exposure to MAc.

We reach a similar conclusion when examining all initial-pH_i/ΔpH_i data pairs in the four protocols in which MAc is the first challenge—that is, MAc_1—experienced by naïve neurons: MAc-MAc, MAc-Ac, MAc-pAC and MAc-pMet↓. The best fit regression line for these data (not shown) has R^2 = 0.00056, indicating no relationship.

Relationship between $(pH_i)_1$ and $(pH_i)_2$

In six of the seven twin-pulse protocols—all except Ac-MAc—we found a positive and significant correlation ($p < 0.001$; not shown) between the pH_i before the first challenge, $(pH_i)_1$, and the pH_i before the second challenge, $(pH_i)_2$. That is, higher $(pH_i)_1$ values correlate with higher $(pH_i)_2$ values.

Twin MAc exposures

In work on cultured mouse HC neurons, Salameh et al. (2014) monitored pH_i while subjecting the cells to two consecutive MAc challenges—MAc_1 and MAc_2—separated by a period of recovery. As set out in Methods (see Definitions), Salameh et al. (2014) characterized cell "state" as resistant vs sensitive based upon the magnitude of $(\Delta pH_i)_1$ during MAc_1 and $(\Delta pH_i)_2$ during MAc_2. Comparing $(\Delta pH_i)_2$ vs the previous $(\Delta pH_i)_1$, those authors also defined neuron "behavior" as "adaptation", "consistency," and "decompensation" based on the position of the neuron on a $[(\Delta pH_i)_1, (\Delta pH_i)_2]$ coordinate system, with respect to the hourglass defined by Equations 1, 2 in Methods.

Salameh et al. worked with mouse (rather than rat) HC neurons, and cultured the HC neurons together with abundant (rather than depleted) astrocytes. In this first Results section, we ask whether the Salameh results for twin MAc pulses are generalizable to the present conditions for rat HC neurons.

Sample pHi records

Figure 3A shows pH_i records—colored blue, green, and red—from three rat HC neurons, each challenged with two consecutive MAc pulses. For the green record, we label [1] $(pH_i)_1$, the pH_i just before MAc_1; [2] $(\Delta pH_i)_1$, the pH_i change

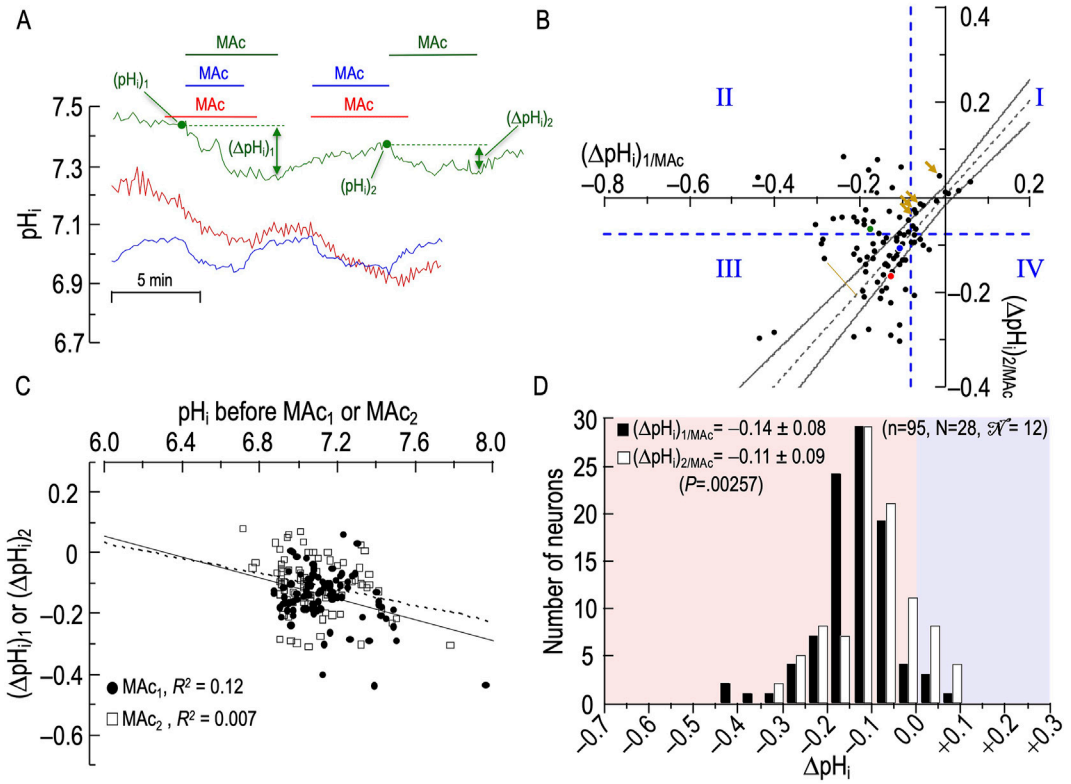

FIGURE 3
Effect of twin exposures to metabolic acidosis (MAc) on pH_i of rat hippocampal neurons **(A)**, examples of pH_i responses of three neurons to twin challenges in which we switched from standard CO_2/HCO_3^- (solution 2, Table 1) to MAc (solution 3, Table 1). Unless otherwise indicated, the extracellular solution was standard CO_2/HCO_3^- (solution 2, Table 1). **(B)**, relationship between the ΔpH_i during the first exposure to MAc—that is, $(\Delta pH_i)_{1/MAc}$—and ΔpH_i during the second exposure to MAc—that is, $(\Delta pH_i)_{2/MAc}$. The vertical dashed blue line is the resistant-sensitive demarcation for MAc_1, and the horizontal dashed blue line is the same for MAc_2. Both demarcations are at $\Delta pH_i/\Delta pH_o$ = 40%. Together, these dashed lines define quadrants Q_I through Q_{IV} and "pH_i states." Because the blue and red dots, representing the blue and red neurons in **(A)**, are in Q_{III}, those neurons are both MAc_1 sensitive and MAc_2 sensitive. Because the green dot is in Q_{II}, the green neuron in panel A is MAc_1 sensitive but MAc_2 resistant. The four bronze arrows indicate four neurons that were MAc resistant in both challenges. The dashed gray line represents the line of identity, for which $(\Delta pH_i)_{1/MAc} = (\Delta pH_i)_{2/MAc}$. The upper and lower bending asymptotes—the hourglass, which defines "pH_i behavior"—represent the confidence interval as described in Methods. Using these criteria, the blue neuron in panel A displays consistency because the blue point in **(B)** lies within the hourglass, that is, $(\Delta pH_i)_2 \cong (\Delta pH_i)_1$. The green neuron displays adaptation because the green point lies above the upper asymptote of the hourglass. The red neuron displays decompensation because the red point lies just below the lower asymptote of the hourglass. **(C)**, dependence of $(\Delta pH_i)_1$ (black circles) or $(\Delta pH_i)_2$ (white squares) on the initial pH_i before MAc_1 and MAc_2, respectively. The solid and dashed lines represent the linear regressions for MAc_1 and MAc_2, respectively. **(D)**, frequency distribution of $(\Delta pH_i)_{1/MAc}$ (black bars) and $(\Delta pH_i)_{2/MAc}$ (white bars) with a pH_i bin width of 0.05 pH units. In the upper left, we report means ± standard deviation as well as the *p*-value (paired t-test, two-tails). In the upper right, we report n, number of neurons; N, number of cover slips; $\mathcal{N}$, number of animals/cultures.

by the end of MAc_1; [3] $(pH_i)_2$, the pH_i just before MAc_2; and [4] $(\Delta pH_i)_2$, the pH_i change by the end of MAc_2. The blue and red[2] pH_i records show neurons with relatively large acidifications during the first MAc exposure (i.e., they are MAc_1 sensitive), and relatively large acidifications during the second MAc exposure (i.e., they are MAc_2 sensitive as well). The green pH_i trace shows a neuron with a relatively large acidification during the first MAc exposure (i.e., it is MAc1 sensitive), but a smaller pH_i change during the second MAc exposure (i.e., it is MAc2 resistant).

Figure 3B is the basis for three analyses, identified below as #1 (State), #2 (Behavior), and #3 ($d_{\pm}$). The first two are based on approaches of Salameh et al. (2014) as defined in Methods. The third is novel to the present paper Figure 3A shows how 95 individual neurons (n = 95, N = 28, $\mathcal{N}$ = 12) respond to MAc_1 and MAc_2. The *x*-axis represents $(\Delta pH_i)_1$ and the *y*-axis, $(\Delta pH_i)_2$. Each of the 95 points represents a separate neuron, with the three colored points representing the three neurons in Figure 3A. Table 2 summarizes some of the statistics from the protocols of Figure 3 through Figure 9.

2 For the neuron represented by the red record, pH_i at the outset of the experiment at first appears to decline and then nearly stabilize just before MAc_1. The pH_i declines are initially slow but continuous throughout the MAc periods—reminiscent of AE3-KO neurons in the study by Salameh et al. (2017). They proposed that, during MAc, AE3 exchanges intracellular HCO_3^- for extracellular Cl^-, which causes (a) an initial rapid fall of pH_i, (b) loads the cell with Cl^-, thereby maintaining $[Cl^-]_i$, thereby (c) maximizing acid extrusion and stabilizing pH_i during the latter portion of the MAc. Thus, AE3 would promote a rapid but limited pH_i decline. A cell with low AE3 activity (or any phenotype that would lower $[Cl^-]_i$) could behave like the red neuron.

TABLE 2 Summary of data sets represented in Figure 3 through Figure 9

Protocol	Figure	Table	n	N	$\mathcal{N}$	$d_{Absolute}$	$d_{\pm}$	Corrected $d_{\pm}$	$\Delta(pH_i)_1$	$\Delta(pH_i)_2$
MAc-MAc	3	3	95	28	12	0.055	+0.024 ± 0.075 (p = .00258)		−0.14 ± 0.08	−0.11 ± 0.09
Ac-MAc	4	4	39	17	10	0.076	+0.015 ± 0.121 (p = .434)		−0.11 ± 0.12	−0.09 ± 0.09
MAc-Ac	5	5	37	13	7	0.107	+0.023 ± 0.138 (p = .309)		−0.11 ± 0.09	−0.07 ± 0.13
pAc-MAc	6	6	47	13	7	0.058	−0.015 ± 0.083 (p = .211)		−0.10 ± 0.10	−0.12 ± 0.10
MAc-pAc	7	7	37	19	6	0.044	+0.020 ± 0.054 (p = .0275)		−0.10 ± 0.10	−0.07 ± 0.06
pMet↓-MAc	8	8	52	17	12	0.078	−0.047 ± 0.082 (p = .000110)	−0.022	−0.04 ± 0.10	−0.11 ± 0.07
MAc-pMet↓	9	9	61	24	9	0.094	+0.094 ± 0.069 (p = 2.28×10^{-15})		−0.07 ± 0.08	−0.06 ± 0.06

[a]Column headings: Figure, Figure number for data set; Table, Table number for data set; n, number of neurons; N, number of cover slips; $\mathcal{N}$, number of culture preparations; $d_{Absolute}$, average absolute (positive) distance from point to line of identity; $d_{\pm}$, mean signed distance from point to line of identity; Corrected $d_{\pm}$, $d_{\pm}$ corrected for shift between $(\Delta pH_i)_{1/pMet\downarrow}$ vs $(\Delta pH_i)_{1/MAc}$, in Figure 8 vs Figure 9; $(\Delta pH_i)_1$, pH_i change during first acid-base challenge; $(\Delta pH_i)_2$, pH_i change during second acid-base challenge. Row headings: MAc, metabolic acidosis; Ac, acidosis (in the nominal absence of CO_2/HCO_3^-); pAc, pure acidosis; pMet↓, pure metabolic down (i.e., decrease in $[HCO_3^-]_o$).

Analysis #1 state

As noted in Methods, we can represent state by the position of a cell with respect to the vertical dashed blue line (the resistant-sensitive demarcation for MAc_1) and the horizontal dashed blue line (the resistant-sensitive demarcation for MAc_2). The two dashed blue lines define four "quadrants", Q_I through Q_{IV}. As we will see below, the position of a neuron in one of the four quadrants describes how the state of the neuron changes[3] (or does not change) in the progression from MAc_1 to MAc_2.

Consistent with our analysis of Figure 1 (a data set of 235 neurons that includes the 95 here), we see here in Figure 3B that a minority of the neurons (19/95 or 20%) lie to the right of the vertical dashed line. That is, according to the definition of Salameh et al. (2014), the state of these neurons during MAc_1 is MAc resistant; the left side of Table 3A provides a numerical summary of these neurons. The majority (80%) of neurons, however, lie to the left of the vertical dashed line; that is, their state is sensitive during MAc_1 (Table 3A, right). The remainder of Table 3 summarizes the state transition from MAc_1 to MAc_2 (Table 3B), the behavior (i.e., adaptation, consistency, decompensation) between MAc_1 and MAc_2 (Table 3C), and the state during MAc_2 (Table 3D). During the second MAc challenge, 33 of 95 or 35% of the neurons lie above the horizontal dashed line in Figure 3B; that is, these neurons are resistant during MAc_2, as also summarized in Table 3D/left. On the other hand, 65% lie below this line (Table 3D/right) and are therefore MAc_2 sensitive. Note that the distribution of MAc-resistant to MAc-sensitive neurons is 35%/65% during MAc_2, compared to 20%/80% during MAc_1. That is, from MAc_1 to MAc_2, we see a general trend toward MAc resistance.

Table 3B traces the fates (i.e., behavior) of the neurons identified as resistant or sensitive during MAc_1:

- Of the 19 neurons identified as resistant during MAc_1, 12 remain resistant during MAc_2. By definition, these 12 MAc_1-resistant/MAc_2-resistant neurons all lie in the first quadrant (Q_I, upper right) in Figure 3B.
- Of the seven previously resistant neurons become sensitive during MAc_2 and therefore lie in Q_{IV} (lower right), which contains all MAc_1-resistant/MAc_2-sensitive neurons.
- Of the 76 neurons identified as sensitive during MAc_1, 55 remain sensitive during MAc_2, and thus lie in Q_{III}, (lower left), which contains all MAc_1-sensitive/MAc_2-sensitive neurons.
- Finally, 21 of the 76 become resistant and thus lie in Q_{II} (upper left), which contains all MAc_1-sensitive/MAc_2-resistant neurons.

Thus, of the 33 neurons resistant during MAc_2 (Table 3D), only 12 were originally resistant in MAc_1, whereas 21 more were sensitive during MAc_1 but became resistant. Similarly, of the 62 neurons identified as sensitive during MAc_2 (Table 3D), 55 were sensitive during MAc_1, and seven others that were resistant during MAc_1 became sensitive. Thus, although shifts in state are not uncommon—the more common being from MAc_1-sensitive to MAc_2-resistant (i.e., Q_{II}) rather than from MAc_1-resistant to MAc_2- sensitive (i.e., Q_{IV})—neurons tend to maintain their resistant/sensitive state-phenotypes between MAc_1 and MAc_2 (i.e., Q_I and Q_{III}).

For the remainder of Results, we present tabular data analogous to that in Table 3 (see Table 4 through Table 9) but limit the presentation to a few salient features in the table legends. Thus, the above presentation of Table 3 serves as a guide for the six later tables.

Analysis #2: Behavior (i.e., hourglass)

The second approach for examining the data in Figure 3B is the hourglass analysis of behavior, introduced by Salameh et al. (2014) and summarized in Methods[4], as well as the legend of Figure 3. Table 3C lists the behaviors of the 95 neurons. For example, of the 12 MAc_1-resistant/MAc_2-resistant neurons that lie in Q_I, four lie above the hourglass (bronze arrows in Figure 3B); that is, their

3 Note that using the quadrants to track the "state" of a neuron from MAc_1 to MAc_2 is not necessarily the same as using the hourglass (discussed below under #2) to define "behavior".

4 See Methods > Definitions > Behavior.

TABLE 3 State and behavior of 95 hippocampal neurons during twin pulses of metabolic acidosis (MAc).

A, state:* MAc_1	19 neurons (20%) = resistant†		76 neurons (80%) = sensitive†		
B, State transition:† $MAc_1 \rightarrow MAc_2$	12 (13%) remain Resistant [Q_I]	7 (7%) become Sensitive [Q_{IV}]	21 (22%) become Resistant [Q_{II}]	55 (58%) remain Sensitive [Q_{III}]	
C, Behavior:‡ $MAc_1 \rightarrow MAc_2$*					Total
Adaptation	4 (4%)	0	20 (21%)	17 (18%)	41 (43%)
Consistency	8 (9%)	3 (3%)	1 (1%)	20 (21%)	32 (34%)
Decompensation	0	4 (4%)	0	18 (19%)	22 (23%)
D, State:† MAc_2 resistant	33 (35%)		MAc2 Sensitive	62 (65%)	

[a]State for pulse 1: resistant neurons are to the right of the vertical dashed blue line; sensitive neurons are to the left.
[b]State for pulse 2, resistant neurons are above the horizontal dashed blue line; sensitive neurons are below.
[c]Behaviors for pulse 1→2 transition: Adaptation (i.e., point is above the hourglass); Consistency (i.e., point is within the hourglass); Decompensation (i.e., point is below the hourglass).
Key points: During MAc_1, most HC, neurons are sensitive, whereas during MAc_2, we observe a trend toward resistance. This shift is associated with an adaptation behavior supported by an overall positive $d\pm$ (see Table 2).
Q, quadrant; Q_I, quadrant I (neurons that are resistant during MAc_1, and remain resistant during MAc_2); Q_{II}, quadrant II (MAc_1 sensitive → MAc_2 resistant); Q_{III}, quadrant III (MAc_1 sensitive → MAc_2 sensitive); Q_{IV}, quadrant IV (MAc_1 resistant → MAc_2 sensitive).

TABLE 4 State and behavior of 39 hippocampal neurons during exposure to extracellular acidosis (Ac) and metabolic acidosis (MAc).

A, state:* Ac_1	13 neurons (33%) = resistant		26 neurons (67%) = sensitive		
B, state transition:† $Ac_1 \rightarrow MAc_2$	7 (18%) remain resistant [Q_I]	6 (15%) become sensitive [Q_{IV}]	11 (28%) become resistant [Q_{II}]	15 (39%) remain sensitive [Q_{III}]	
C, Behavior:‡ $Ac_1 \rightarrow MAc_2$*					Total
Adaptation	2 (5%)	0	11 (28%)	2 (5%)	15 (38%)
Consistency	3 (8%)	0	0	5 (13%)	8 (21%)
Decompensation	2 (5%)	6 (15%)	0	8 (21%)	16 (41%)
D, State:† MAc_2 Resistant	18 (46%)[Δ]		MAc_2 Sensitive	21 (54%)[Δ]	

[a]State for pulse 1: resistant neurons are to the right of the vertical dashed blue line; sensitive neurons are to the left.
[b]State for pulse 2, resistant neurons are above the horizontal dashed blue line; sensitive neurons are below.
[c]Behaviors for pulse 1→2 transition: Adaptation (i.e., point is above the hourglass); Consistency (i.e., point is within the hourglass); Decompensation (i.e., point is below the hourglass).
Q, quadrant; Q_I, quadrant I (neurons that are "resistant" during Ac_1, and remain resistant during MAc_2); Q_{II}, quadrant II (Ac_1 sensitive → MAc_2 resistant); Q_{III}, quadrant III (Ac_1 sensitive → MAc_2 sensitive); Q_{IV}, quadrant IV (Ac_1 resistant → MAc_2 sensitive).
[Δ]**Key points:** In this Ac-MAc, protocol, 46% of the neurons are MAc_2 resistant vs only 35% in the MAc-MAc, protocol (see Table 3D). A two-sample Z-test for proportions reveals that 35% MAc_2 resistance in MAc-MAc, is not significantly different from 46% in Ac-MAc ($p = 0.216$).

behavior is adaptation. The other eight neurons lie within the hourglass; their behavior is consistency. None of these 12 neurons lie below the hourglass; that is, none has a decompensation behavior.

In the rightmost column of Table 3C, we summarize the behaviors of all 95 neurons. For example, 41 of 95 neurons or 43%—including the one represented by the green point here and the green record in panel A—lie above the hourglass. These 41 neurons have an adaptation behavior. In fact, seven of these 41 points lie at least ~0.02 pH units above the *x*-axis; that is, these neurons adapted to such an extent that they exhibit a frank alkalinization during MAc_2. Table 3C also shows that 32 of 95 or 34% of the neurons—including the one represented by the blue point and record—lie within the hourglass; that is, their behavior is consistent between MAc_1 and MAc_2. Finally, 22 of 95 or 23% of the neurons—including the one represented by the red point and record—lie below the hourglass; that is, these neurons exhibit a decompensation behavior between MAc_1 and MAc_2. Note that four of these decompensating neurons were MAc_1 resistant but MAc_2 sensitive, whereas 18 were MAc_1 sensitive and remained sensitive during MAc_2 (albeit with a greater magnitude of ΔpH_i).

Analysis #3: $d_{\pm}$

The third analysis, which we introduce in the present paper is actually two closely related calculations. In the first, we compute the mean absolute distance ($d_{Absolute}$) between each neuron-point to the nearest point[5] on the line of identity (LOI). All $d_{Absolute}$ values are positive. We indicate this relationship in Figure 3B with the gold line segment between one neuron in Q_{III} and the LOI. For each protocol, the mean $d_{Absolute}$ value is in the seventh column of Table 2. In the second calculation, we compute the mean signed distance ($d_{\pm}$). Individual values are positive if the corresponding point lies to the upper left of the LOI (as for the gold line segment in Figure 3B)—this is analogous to adaptation behavior, but does not take into account the confidence interval represented by the hourglass. Individual values are negative if the corresponding point lies to the lower right of the LOI analogous to decompensation behavior. Mean $d_{\pm}$ values for each protocol are in the eighth column of Table 2. For this MAc-MAc protocol, the mean $d_{\pm}$ is ~ +0.024 (p = .00258; Table 2, row 1), which indicates that the average point is significantly to the upper-left of the LOI, consistent with an overall tendency toward an adaptation behavior.

ΔpH_i vs initial pH_i

To determine whether the pH_i just before MAc_1 or MAc_2 correlates with the ΔpH_i during the subsequent MAc, in Figure 3C we plot ΔpH_i vs the initial pH_i for both MAc pulses. As described above for Figure 2B, taking all 95 points together, we find the overall correlation strength to be "absent" (see Methods[6]), both between $(\Delta pH_i)_1$ and $(pH_i)_1$ (filled circles; R^2 = 0.12), and between $(\Delta pH_i)_2$ and $(pH_i)_2$ (open squares; R^2 = 0.007).

Returning to Figure 3A, we see that the red record is from a neuron in which $(\Delta pH_i)_1$ was relatively large, and for which the pH_i recovery from MAc_1 was small, so that $(pH_i)_2$ was substantially lower than $(pH_i)_1$. Indeed, our analysis (not shown) of the 95 neurons in Figure 3 shows a weak correlation (R^2 = 0.36) between $(\Delta pH_i)_1$ and the difference $[(pH_i)_2 - (pH_i)_1]$. That is, as the acidification during MAc_1 increases in magnitude, $(pH_i)_2$ tends to fall increasingly below $(pH_i)_1$.

Frequency distributions

Figure 3D shows the frequency distributions of ΔpH_i for both MAc_1 and MAc_2 and reveals a statistically significant shift to the right (i.e., smaller negative ΔpH_i values, larger positive ones) between MAc_1 and MAc_2. This result is consistent with an overall trend to adaptation and the observed positive value of $d_{\pm}$. Note that this traditional histogram cannot capture the rich diversity among neurons, as revealed in Figures 3B, C and Table 3.

Summary of MAc-MAc

Most rat HC neurons have a MAc-sensitive "state", both during MAc_1 and MAc_2 (Q_{III}). From MAc_1 to MAc_2, the neurons tend to show adaptation-like "behavior", being both above the hourglass and having a positive $d_{\pm}$.

Extracellular acidosis in the absence of CO_2/HCO_3^- (Ac) and then MAc

To begin exploring the role of ΔpH_o *per se* in producing the ΔpH_i observed during MAc, we examine neurons exposed to a CO_2/HCO_3^--free solution at pH 7.40 (solution 1, Table 1) and then subject the neurons—in the continuing absence of CO_2/HCO_3^-—to extracellular acidosis (Ac; pH_o 7.20; solution 4, Table 1). To compare this Ac-induced pH_i response with our previous MAc data, we return the neurons to the pH-7.4 solution 1, then switch to our standard CO_2/HCO_3^- solution (solution 2, Table 1), and then finally impose a standard MAc (solution 3, Table 1).

Nomenclature

We do not expect the response to Ac—or other single-parameter challenges presented later—to be the same as the response to MAc. Ac, for one, occurs in the nominal absence of CO_2 and HCO_3^-, where minimal CO_2 or HCO_3^- is present for sensing or effector mechanisms (e.g., transport of HCO_3^--related species). Moreover, we do not expect the response to the twin challenge Ac-MAc—and other twin challenges presented later—to be the same as the response to MAc-MAc. Nevertheless, for the sake of consistent comparisons, we analyze them all as we do for MAc-MAc. Thus, we will use terms like "resistant" and "adaptation" the same way as we use them for MAc and MAc-MAc, respectively, understanding that this use is for our convenience and does not necessarily imply equivalence of the physiological challenges.

Sample pH_i records

Figure 4A shows the pH_i responses of three neurons to the aforementioned protocol. We focus first on the blue record. Imposing Ac_1 (first challenge) produces a slow decrease in pH_i, the final magnitude of which is $(\Delta pH_i)_{1/Ac}$. Returning pH_o to 7.40 produces a slow pH_i recovery, presumably due to Na-H exchange (Baxter and Church, 1996; Bevensee et al., 1996). Adding CO_2/HCO_3^- (downward blue arrow) produces a rapid pH_i decrease due to CO_2 influx, followed by a brisk pH_i recovery due to acid extrusion mediated to some extent by Na-H exchangers, but predominantly by Na^+-coupled HCO_3^- transporters (Schwiening and Boron, 1994; Baxter and Church, 1996; Bevensee et al., 1996). Here, the evidence that HCO_3^- transport is dominant is the far more rapid pH_i-recovery in the presence of CO_2/HCO_3^-, even though total intracellular buffering power must have been far higher in CO_2/HCO_3^- (Roos and Boron, 1981; Boron, 2004). The subsequent MAc_2, like the preceding Ac_1, produces a slow pH_i decline; the pH_i change—$(\Delta pH_i)_{2/MAc}$—is approximately the same magnitude as $(\Delta pH_i)_{1/Ac}$.

The green and red traces in Figure 4A represent two other neurons. Note that, whereas the pH_i response to MAc generally results in a clear shift in steady-state pH_i (see Figure 3A), the response to Ac often results in a continuous downward drift in pH_i. Thus, our $(\Delta pH_i)_{1/Ac}$ values do not necessarily reflect a shift in

5 The line segment between the point and the line of identity is, by definition, orthogonal to the line of identity. Because the *x*-axis scale in Figure 3B is slightly smaller than the *y*-axis scale, the gold-colored line segment is not quite orthogonal to the dashed line of identity.

6 Methods > Data analysis and statistics.

10.3389/fphys.2024.1434359

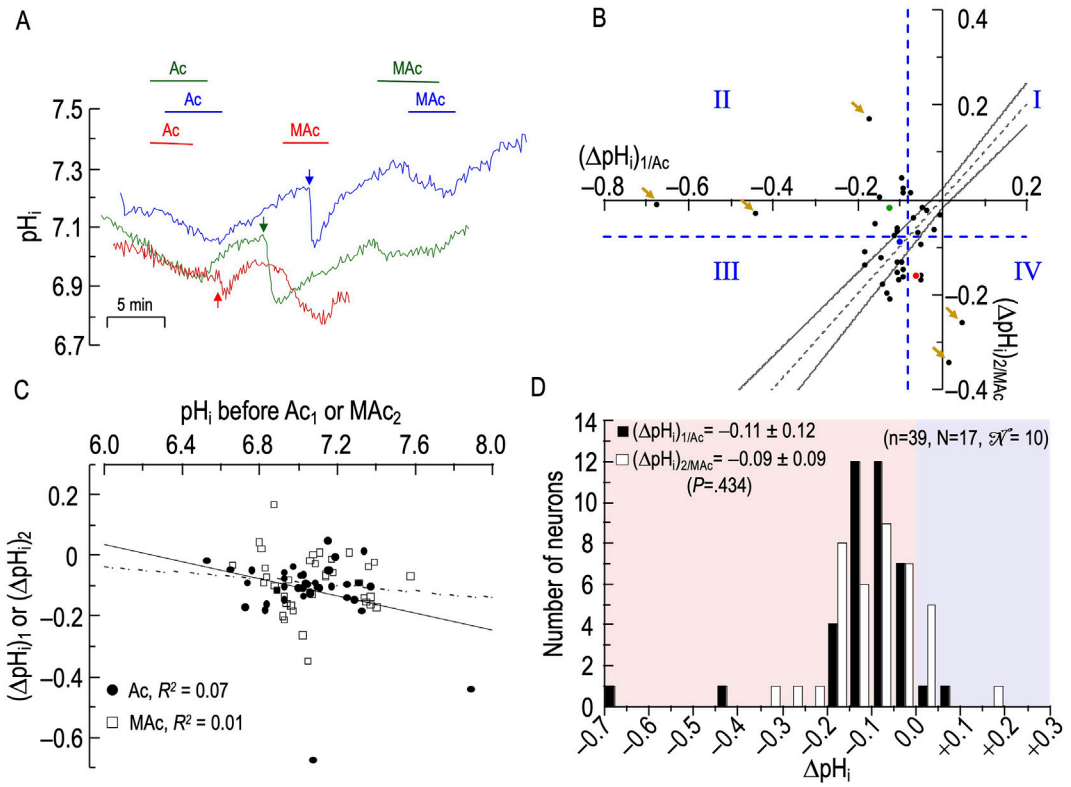

FIGURE 4
Effect extracellular acidosis (Ac) followed by metabolic acidosis (MAc) on the pH_i of rat hippocampal neurons **(A)**, examples of the pH_i responses in three hippocampal neurons to an exposure to Ac (solution 4, Table 1) and then to MAc (solution 3, Table 1). Before the arrows, unless otherwise indicated, the bath solution was our standard nominally CO_2/HCO_3^--free solution (solution 1, Table 1). After the arrows, unless otherwise indicated, the bath solution was standard CO_2/HCO_3^- (solution 2, Table 1). **(B)**, relationship between the ΔpH_i during exposure to Ac—that is, $(\Delta pH_i)_{1/Ac}$—and ΔpH_i during exposure to MAc—that is, $(\Delta pH_i)_{2/MAc}$. The horizontal and vertical dashed blue lines are the resistant-sensitive demarcations that define quadrants I–IV and "pH_i states" (see Figure 3). The blue dot that represents the blue neuron in panel A is in Q_{III} (i.e., neuron is both Ac_1 sensitive and MAc_2 sensitive). The green dot is in Q_{II} (i.e., green neuron in panel A is Ac_1 sensitive but MAc_2 resistant). The red dot is in Q_{IV} (i.e., red neuron in panel A is Ac_1 resistant but MAc_2 sensitive). The five bronze arrows indicate neurons that are particularly distant from the hourglass. Moreover, all five are either near or paradoxically above the *x*-axis, or to the right of the *y*-axis. The dashed gray line is the line of identity; the gray hourglass represents the confidence interval and defines "pH_i behavior" (see Figure 3). Because the blue point lies within the hourglass, the behavior of the blue neuron is consistency. The green point lies above the upper asymptote of the hourglass; the behavior is adaptation. The red neuron lies below the lower asymptote of the hourglass; the behavior is decompensation. **(C)**, dependence of $(\Delta pH_i)_1$ (black circles) on the initial pH_i before Ac_1, which we refer to as $(\Delta pH_i)_{1/Ac}$, or dependence of $(\Delta pH_i)_2$ (white squares) on the initial pH_i before and MAc_2, which we refer to as $(\Delta pH_i)_{2/MAc}$. The solid and dashed lines represent the linear regressions for Ac_1 and MAc_2, respectively. **(D)**, frequency distribution of $(\Delta pHi)_{1/Ac}$ (black bars) and $(\Delta pHi)_{2/MAc}$ (white bars) with a pH_i bin width of 0.05 pH units. In the upper left, we report means ± standard deviation as well as the *p*-value (paired t-test, two-tails). n, number of neurons; N, number of cover slips; $\mathcal{N}$, number of animals/cultures.

steady-state pH_i *per se*, but an evolving pH_i change over a time period similar to that in MAc challenges. We present these Ac_1 data so that the reader may be aware that pH_o changes under non-physiological conditions often lead to unexpected consequences. The pH_i data for MAc_2 are rather nominal except for the red trace, which may have been drifting downward just before the MAc_2 challenge.

Analyses #1–3

Figure 4B and Table 4 summarize state and behavior for the full Ac-MAc dataset (n = 39, N = 17, $\mathcal{N}$ = 10).[7] Figure 4B reveals that most neurons have relatively low absolute values of $(\Delta pH_i)_{1/Ac}$ and $(\Delta pH_i)_{2/MAc}$, and most tend to cluster near the hourglass. The notable exceptions are five neurons (bronze arrows) that are rather distant from the hourglass, three neurons in Q_{II}, and two others in Q_{IV}.

The blue point, which corresponds to the neuron represented by the same color in Figure 4A, lies in Q_{III} (i.e., its "state" fulfills the MAc criteria for Ac_1 sensitivity and is MAc_2 sensitive) and falls within the hourglass, near the LOI (its "behavior" fulfills the MAc-MAc criteria for consistency (see Figures 3A,B).

The green point lies in Q_{II} (i.e., its states are Ac_1 sensitive but MAc_2 resistant), and above the hourglass (i.e., behavior is adaptation).

The red point lies in Q_{IV} (i.e., states are Ac_1 resistant and MAc_2 sensitive), and just outside of the lower bound of the hourglass (i.e., behavior is decompensation).

7 For an example of how to interpret this table, see the analogous presentation in the MAc-MAc section.

The $d_{\pm}$ of +0.015 (Table 2, row 2) is not significantly different from zero, consistent with our subjective impression of a general clustering near the hourglass.

ΔpH_i vs initial pH_i

Figure 4C shows that the correlation strengths, taking all 39 points together, were "absent" for both $(\Delta pH_i)_{1/Ac}$ vs $(pH_i)_1$, and for $(\Delta pH_i)_{2/MAc}$ vs $(pH_i)_2$.

Frequency distributions

Figure 4D shows the frequency distributions of ΔpH_i for both Ac_1 and MAc_2. Unlike the situation for MAc-MAc (see Figure 3D), $(\Delta pH_i)_2$ is not significantly different from $(\Delta pH_i)_1$ in the Ac-MAc protocol. Note that the MAc response during pulse two in the Ac-MAc protocol $(\Delta pH_i)_{2/MAc} = -0.09 \pm 0.09$ (see Figure 4D) is not significantly different from its counterpart in the MAc-MAc protocol ($(\Delta pH_i)_{2/MAc} = -0.11 \pm 0.09$, $p = 0.333$, unpaired t-test, in Figure 3D).

Summary of Ac-MAc

Ac_1 often causes a slow, continuing decline in pH_i, and—compared to MAc-MAc—has a negligible effect on $(\Delta pH_i)_{2/MAc}$.

MAc and then Ac

In this new experimental series, we reverse the order of the challenges in Figure 4, exposing the neurons first to MAc then to Ac (in absence of CO_2/HCO_3^-).

Sample pH_i records

Figure 5A shows three examples of pH_i responses of HC neurons during an exposure to MAc and then to Ac. Focusing first on the blue record, we see that the neuron responds to MAc_1 with a modest acidification. Unexpectedly, the removal of CO_2/HCO_3^- (blue arrow in Figure 5A; solution 2 → solution 1; Table 1) does not elicit the usual abrupt pH_i increase due to CO_2 efflux. It is possible that strong AE3 activity (Salameh et al., 2017) produced a HCO_3^- efflux that nullified the pH_i effects of CO_2 efflux. In the continued absence of CO_2/HCO_3^-, imposing Ac_2 produces a slow but sustained pH_i decrease. It is not clear whether this pH_i decrease would have subsided, had we extended the Ac exposure.[8] Restoring pH_o 7.40 produces the expected pH_i recovery.

The neuron represented by the green record has a larger response to MAc_1, a small pH_i recovery after removal of MAc, and a modest pH_i increase due to CO_2 efflux upon removal of CO_2/HCO_3^-. Ac_2 paradoxically causes a frank alkalinization. The red record slowly approaches a stable pH_i in CO_2/HCO_3^-, and MAc_1 elicits only a small pH_i decrease, the magnitude of which we may have slightly underestimated because pH_i may not have been entirely stable before the MAc_1. Nevertheless, the return to pH_o 7.40 in CO_2/HCO_3^- elicits a robust pH_i increase. The subsequent removal of CO_2/HCO_3^- produces a very large pH_i increase (perhaps reflecting a low AE3 activity), and the Ac_2 challenge leads to a slow, seemingly interminable pH_i decrease. Removing Ac_2 does not elicit a pH_i recovery, at least in the brief time allotted. We present these Ac_2 data so that the reader may be aware that pH_o changes under non-physiological conditions often lead to unexpected consequences.

Analyses #1–3

Figure 5B and Table 5 summarize state and behavior for the full MAc-Ac dataset (n = 37, N = 13, $\mathcal{N}$ = 7). Figure 5B reveals a very different pattern from Figure 4B, with many neurons deviating markedly from the hourglass. Most neurons lie in band that runs from the upper-left (Q_{II}) to the lower-right (Q_{IV}), and thus range in behavior from strong adaptation to strong decompensation.

The blue point lies in Q_{III} (i.e., states are MAc_1 and Ac_2 sensitive), and within the hourglass (i.e., behavior is consistency).

The green point lies in Q_{II} (i.e., states are MAc_1 sensitive but Ac_2 resistant), and well above the hourglass (i.e., behavior is adaptation). In fact, this is one of eight neurons that fall at least 0.02 above the x-axis. This frequency of frank alkalinization during Ac_2 (8 of 37 neurons = 19%) is far higher than for Ac_1 in Figure 4B (2 of 39 = 5% are to the right of the y-axis). Thus, the MAc_1 pretreatment promotes paradoxical alkalinization during Ac_2—a theme that repeats itself below when MAc_1 precedes pAc_2 or $pMet\downarrow_2$. Because the extracellular solution is nominally free of CO_2/HCO_3^-, Na-H exchange most likely mediates this paradoxical alkalization, to the extent that it is opposed by background acid loading (Bevensee and Boron, 2013).

The red point in Figure 5B lies in Q_{IV} (i.e., states are MAc_1 resistant but Ac_2 sensitive), and below the hourglass (i.e., behavior is decompensation).

The $d_{\pm}$ of +0.023 (Table 2, row 3) reveals a trend toward adaptation. However, this is not significantly different from zero because the SD of 0.138 is so large, consistent with our subjective impression of a broad dispersion of neurons from Q_{II} to Q_{IV}.

ΔpH_i vs initial pH_i

Figure 5C reveals a correlation strength, taking all 52 points together, of "absent" between $(\Delta pH_i)_{1/MAc}$ and $(pH_i)_1$. The weak correlation strength between $(\Delta pH_i)_{2/Ac}$ and $(pH_i)_2$ is consistent with a greater acidification for neurons with a higher pre-Ac_2 pH_i.

Frequency distributions

Figure 5D shows the frequency distributions of ΔpH_i for both MAc_1 and Ac_2. Although the Ac_2 distribution tends to shift to the right, the difference is not statistically significant.

Summary of MAc-Ac

With some neurons, Ac_2 causes seemingly continuous pH_i decreases and strong decompensating behavior. In others, perhaps primed by the preceding MAc_1, Ac_2 leads to strong adaptive behavior and often frank, paradoxical alkalinization.

An isolated pH_o decrease (pAc) and then MAc

A limitation of the Ac-MAc and MAc-Ac studies is that the absence of CO_2/HCO_3^- during the fall of pH_o could limit both the

8 The duration of experiments is limited by the health of the neuron, which we judge by $-k_{440}$.

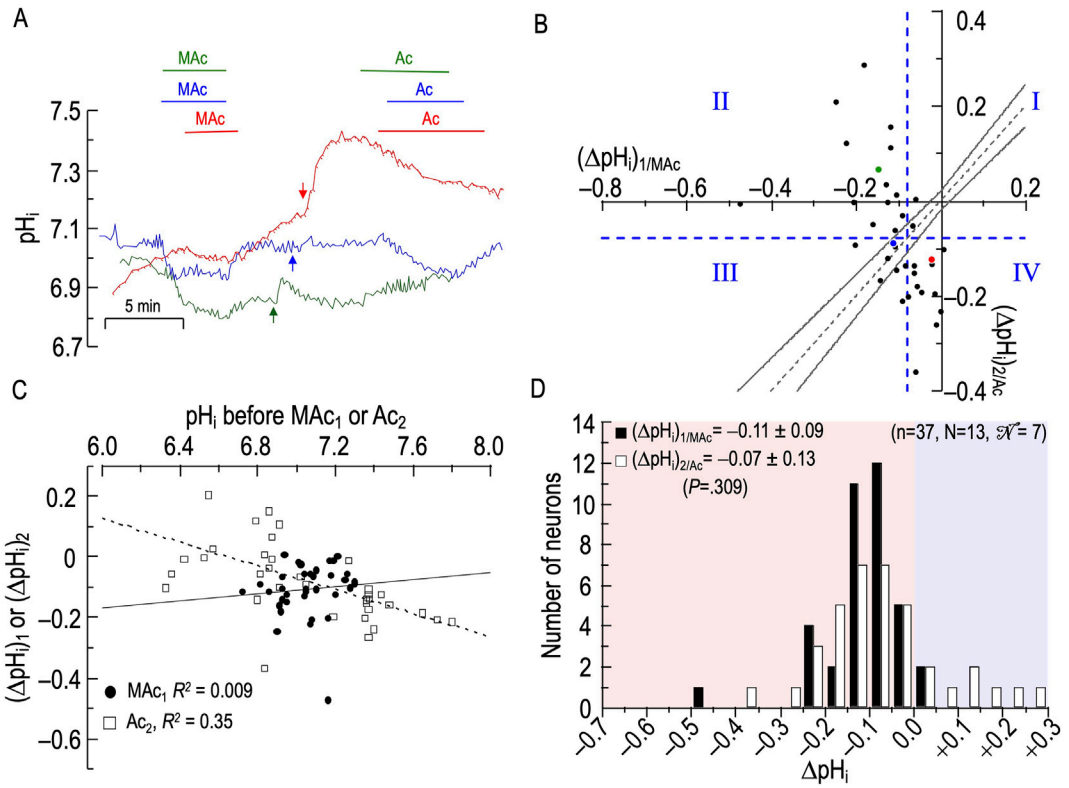

FIGURE 5
Effect of metabolic acidosis (MAc) followed by extracellular acidosis (Ac) on the pH_i of rat hippocampal neurons **(A)**, examples of the pH_i responses in three hippocampal neurons to an exposure to MAc (solution 3, Table 1) and then to Ac (solution 4, Table 1). Before the arrows, unless otherwise indicated, the bath solution was standard CO_2/HCO_3^- (solution 2, Table 1 After the arrows, unless otherwise indicated, the bath solution was our standard nominally CO_2/HCO_3^--free solution (solution 1; Table 1). **(B)**, relationship between the ΔpH_i during exposure to MAc—that is, $(\Delta pH_i)_{1/MAc}$—and ΔpH_i during exposure to Ac—that is, $(\Delta pH_i)_{2/Ac}$. The horizontal and vertical dashed blue lines are the resistant-sensitive demarcations that define quadrants I–IV and "pH_i states" (see Figure 3). The blue dot that represents the blue neuron in panel A is in Q_{III} (i.e., neuron is both MAc_1 sensitive and Ac_2 sensitive). The green dot is in Q_{II} (i.e., green neuron in panel **(A)** is MAc_1 sensitive but Ac_2 resistant). The red dot is in Q_{IV} (i.e., red neuron in panel **(A)** is MAc_1 resistant but Ac_2 sensitive). Note that, for the green neuron, $(\Delta pH_i)_{2/Ac}$ is paradoxically positive. The dashed gray line is the line of identity; the gray hourglass represents the confidence interval and defines "pH_i behavior" (see Figure 3). Because the blue point lies within the hourglass, the behavior of the blue neuron is consistency. The green point lies above the upper asymptote of the hourglass; the behavior is adaptation. The red neuron lies below the lower asymptote of the hourglass; the behavior is decompensation. **(C)**, dependence of $(\Delta pH_i)_1$ (black circles) on the initial pH_i before MAc_1, which we refer to as $(\Delta pH_i)_{1/MAc}$, or dependence of $(\Delta pH_i)_2$ (white squares) on the initial pH_i before and Ac_2, which we refer to as $(\Delta pH_i)_{2/Ac}$. The solid and dashed lines represent the linear regressions for MAc_1 and Ac_2, respectively. **(D)**, frequency distribution of $(\Delta pH_i)_{1/MAc}$ (black bars) and $(\Delta pH_i)_{2/Ac}$ (white bars) with a pH_i bin width of 0.05 pH units. In the upper left, we report means ± standard deviation as well as the *p*-value (paired t-test, two-tails). n, number of neurons; N, number of cover slips; $\mathcal{N}$, number of animals/cultures.

sensor and effector arms of any cellular response. To gain further understanding on the behavior of HC neurons during extracellular acid-base challenges, in the remainder of the present paper we exploit CO_2/HCO_3^- out-of-equilibrium solutions to modify only one parameter of the Henderson-Hasselbalch equation. First, we use OOE technology to lower pH_o to 7.20—the same acidification that we achieve during MAc—while maintaining a stable $[CO_2]_o$ and $[HCO_3^-]_o$. This pure acidosis protocol begins with neurons bathed in our standard CO_2/HCO_3^- solution, followed by challenges first with pAc (solution 5, Table 1) and then with MAc.

Sample pH_i records

Figure 6A shows three pH_i responses of HC neurons. The blue trace represents a neuron with modest acidification responses to pAc and MAc.

The green trace represents a neuron in which pAc_1 elicits a modestly rapid pH_i decline that shows no sign of abating. The removal of the pAc challenge, rather than heralding a pH_i recovery, initially produces an even more rapid acidification (first green arrow); we observed this pattern, though less dramatically, in four other neurons. Eventually, pH_i spontaneously reverses direction and rises fairly rapidly (second green arrow); we observed this pattern only in this neuron. Finally, the subsequent MAc_2 challenge in the green neuron now elicits only a small pH_i decrease. It is possible that the spontaneous reversal of the pH_i decline (green arrow) is adaption in the making.

Finally, the red trace represents a neuron that displays a small acidification during pAc_1 but acidifies markedly during the subsequent MAc_2.

Analyses #1–3

Figure 6B and Table 6 summarize state and behavior for the full pAc-MAc dataset (n = 47, N = 13, $\mathcal{N}$ = 7). Two characteristics of Figure 6B are noteworthy. First, most of the points lie to the right of the vertical dashed blue line. That is, during pAc_1, most neurons fulfill the

TABLE 5 State and behavior of 37 hippocampal neurons during exposure to metabolic acidosis (MAc) and extracellular acidosis (Ac).

A, state:* MAc_1	16 neurons (43%) = resistant		21 neurons (57%) = sensitive		
B, state transition:† $MAc_1 \rightarrow Ac_2$	3 (8%) remain resistant [Q_I]	13 (35%) become sensitive [Q_{IV}]	9 (24%) become resistant [Q_{II}]	12 (33%) remain sensitive [Q_{III}]	
C, Behavior:‡ $MAc_1 \rightarrow Ac_2$*					Total
Adaptation	1 (3%)	0	9 (24%)	6 (16%)	16 (43%)
Consistency	2 (5%)	0	0	4 (11%)	6 (16%)
Decompensation	0	13 (35%)	0	2 (6%)	15 (41%)
D, State:† Ac_2 Resistant	12 (32%)		Ac_2 Sensitive		25 (66%)

[a]State for pulse 1: resistant neurons are to the right of the vertical dashed blue line; sensitive neurons are to the left.
[b]State for pulse 2, resistant neurons are above the horizontal dashed blue line; sensitive neurons are below.
[c]Behaviors for pulse 1→2 transition: Adaptation (i.e., point is above the hourglass); Consistency (i.e., point is within the hourglass); Decompensation (i.e., point is below the hourglass). Q, quadrant; Q_I, quadrant I (neurons that are resistant during MAc_1, and remain "resistant" during Ac_2); Q_{II}, quadrant II (MAc_1 sensitive → Ac_2 resistant); Q_{III}, quadrant III (MAc_1 sensitive → Ac_2 sensitive); Q_{IV}, quadrant IV (MAc_1 resistant → Ac_2 sensitive).
Key points: (1) Of the 16 MAc_1-resistant neurons (row A), 13 fulfill the criteria for decompensation in the transition to Ac_2. (2) Of the 16 neurons with an adaptation behavior in the transition to Ac_2 (row C), 15—including all eight neurons with a paradoxical alkalinizing response in Ac_2—were MAc_1 sensitive.

MAc_1 criterion for a resistant state. Second, most points lie barely above, within, or below the hourglass. That is, their behavior tends to be consistency or decompensation. Very few neurons (e.g., the green point) display adaptation behavior, and none lie above the *x*-axis.

The blue point lies in Q_{III} (i.e., states are pAc_1 and MAc_2 sensitive), and nearly on the gray dashed line within the hourglass (i.e., behavior is consistency).

The green point lies in Q_{II} (i.e., states are pAc_1 sensitive but MAc_2 resistant), and well above the hourglass (i.e., behavior is adaptation).

The red point lies in Q_{III}, just to the left of the vertical dashed blue line (i.e., states are barely pAc_1 sensitive but solidly MAc_2 sensitive), and below the hourglass (i.e., behavior is decompensation).

Although the mean $d_{\pm}$ of −0.015 (Table 2, row 4) trends toward decompensation, this value is not significantly different from zero.

ΔpH_i vs initial pH_i

Figure 6C reveals correlation strengths, taking all 47 points together, of "absent" both between $(\Delta pH_i)_{1/pAc}$ and $(pH_i)_1$, and between $(\Delta pH_i)_{2/MAc}$ and $(pH_i)_2$.

Frequency distributions

Figure 6D summarizes the distribution of ΔpH_i during the two conditions, and shows that, although we see a tendency for a leftward shift during the second challenge, $(\Delta pH_i)_{2/MAc}$ is not significantly different from$(\Delta pH_i)_{1/pAc}$.

Summary of pAc-MAc

pAc_1 generally produces a small acidification (resistant "state"), followed during MAc_2 by a trend toward decompensation.

MAc and then pAc

In this experimental series, we invert the sequence of exposure from the previous protocol, challenging neurons first with MAc then with pAc.

Sample pH_i records

Figure 7A shows three pH_i responses of HC neurons. The blue pH_i trace represents a neuron that exhibits almost no change in pH_i during MAc_1 exposure, and acidifies only slightly during pAc_2. The green trace reflects large acidifications during both MAc_1 and, to a lesser extent, pAc_2. Finally, the red pH_i trace reports only a small acidification during MAc_1 but a much larger one during pAc_2.

Analyses #1–3

Figure 7B and Table 7 summarize state and behavior for the full MAc-pAc dataset (n = 37, N = 18, $\mathcal{N}$ = 6). In contrast to pAc-MAc, for which Figure 6B gives the subjective impression of many neurons lying below the hourglass, MAc-pAc gives a different impression, with most points line in or near the hourglass ~40% of neurons lying above the hourglass (i.e., adaptation "behavior").

The blue point lies in Q_I (i.e., states are both MAc_1 and pAc_2 resistant), and virtually on the LOI within the hourglass (i.e., behavior is consistency).

The green point lies in Q_{III} (i.e., states are both MAc_1 and pAc_2 sensitive), and above the hourglass (i.e., behavior is adaptation).

The red point lies on the Q_I/Q_{IV} boundary (i.e., states are MAc_1 resistant and barely pAc_2 resistant), and just below the hourglass (i.e., behavior is decompensation).

Consistent with our subjective impression of a predominance of adaptation (i.e., a plurality of neurons lying above the hourglass), the mean $d_{\pm}$ is +0.020 (Table 2, row 5), a value significantly different from zero (p = .0275).

ΔpH_i vs initial pH_i

Figure 7C shows correlation strengths, taking all 37 points together, of "absent", both for $(\Delta pH_i)_1$ vs $(pH_i)_1$, and for $(\Delta pH_i)_2$ vs $(pH_i)_1$.

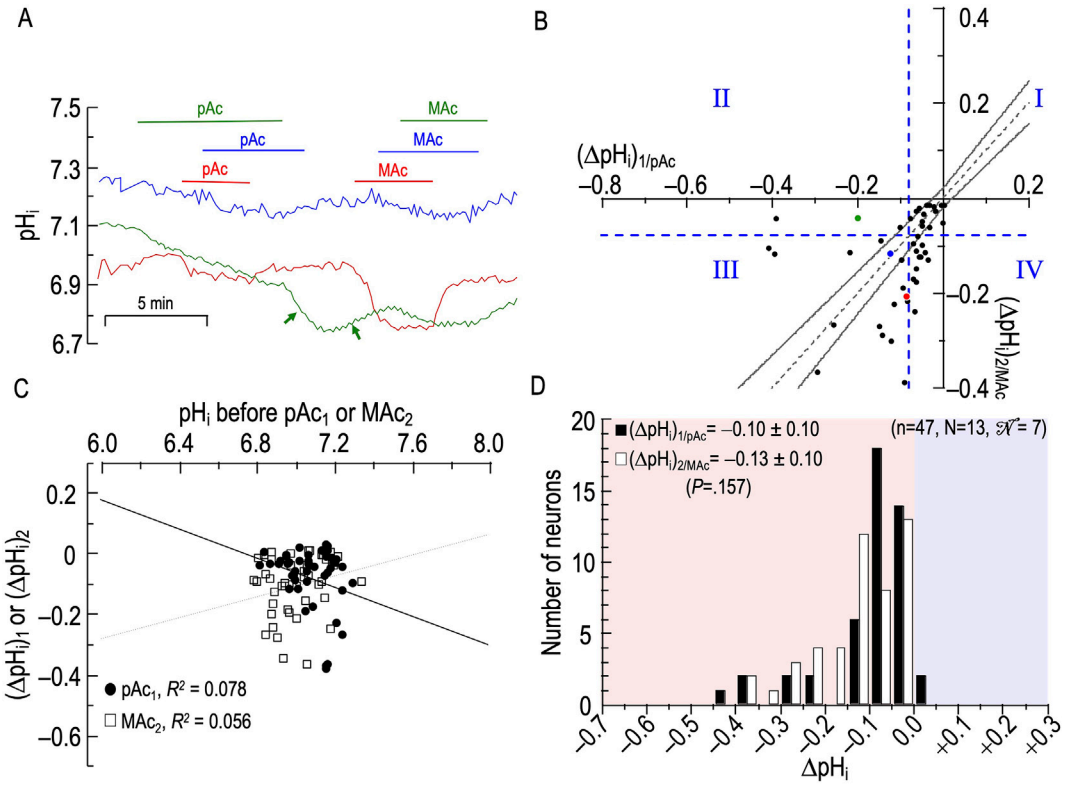

FIGURE 6
Effect of an isolated decrease of pH_o (pAc) followed by metabolic acidosis (MAc) on the pH_i of rat hippocampal neurons **(A)**, examples of the pH_i responses in three hippocampal neurons to an exposure to pAc (solution 5, Table 1), and then to MAc (solution 3, Table 1). Unless otherwise indicated, the bath solution was standard CO_2/HCO_3^- (solution 2, Table 1). The green arrows following pAc removal indicate an initial anomalous pH_i decrease (left) followed by the expected but delayed pH_i increase (right). **(B)**, relationship between the ΔpH_i during exposure to pAc—that is, $(\Delta pH_i)_{1/pAc}$—and ΔpH_i during exposure to MAc—that is, $(\Delta pH_i)_{2/MAc}$. The horizontal and vertical dashed blue lines are the resistant-sensitive demarcations that define quadrants I–IV and "pH_i states" (see Figure 3). The blue dot that represents the blue neuron in panel A is in Q_{III} (i.e., neuron is both pAc_1 sensitive and MAc_2 sensitive). The green dot is in Q_{II} (i.e., green neuron in panel A is pAc_1 sensitive but MAc_2 resistant). Because the red dot is slightly to the left of the vertical dashed blue line, it is in Q_{IV} (i.e., red neuron in panel A is both pAc_1 sensitive and MAc_2 sensitive). The dashed gray line is the line of identity; the gray hourglass represents the confidence interval and defines "pH_i behavior" (see Figure 3). Because the blue point lies within the hourglass, the behavior of the blue neuron is consistency. The green point lies above the upper asymptote of the hourglass; the behavior is adaptation. The red neuron lies below the lower asymptote of the hourglass; the behavior is decompensation. **(C)**, dependence of $(\Delta pH_i)_1$ (black circles) on the initial pH_i before pAc_1, which we refer to as $(\Delta pH_i)_{1/pAc}$, or dependence of $(\Delta pH_i)_2$ (white squares) on the initial pH_i before and MAc_2, which we refer to as $(\Delta pH_i)_{2/MAc}$. The solid and dashed lines represent the linear regressions for pAc_1 and MAc_2, respectively. **(D)**, frequency distribution of $(\Delta pH_i)_{1/pAc}$ (black bars) and $(\Delta pH_i)_{2/MAc}$ (white bars) with a pH_i bin width of 0.05 pH units. In the upper left, we report means ± standard deviation as well as the *p*-value (paired t-test, two-tails). N, number of neurons; N, number of cover slips; $\mathcal{N}$, number of animals/cultures.

Frequency distributions

Figure 7D shows that the mean $(\Delta pH_i)_{2/pAc}$ is less than the mean $(\Delta pH_i)_{1/MAc}$, and that the difference is statistically significant.

Summary of MAc-pAc

Following MAc_1, pAc_2 tends to produce relatively small acidifications.

An isolated decrease in $[HCO_3^-]_o$ (pMet↓) and then MAc

In the two previous experimental series, we explored the effects of an isolated decrease of pH_o—one component of MAc—on neuronal pH_i. In this and the next section, we investigate the effects of the other component of MAc, an isolated decrease of $[HCO_3^-]_o$. Our approach is to use an OOE CO_2/HCO_3^- solution to keep $[CO_2]_o$ and pH_o constant as we lower $[HCO_3^-]_o$ to the same extent as we would in a MAc solution. This pure metabolic/decreasing $[HCO_3^-]_o$ (pMet↓) protocol begins with neurons bathed in our standard CO_2/HCO_3^- solution, followed by two challenges, pMet↓ (solution 6, Table 1) and then MAc.

Sample pH_i records

Figure 8A shows three responses of HC neurons. The blue trace represents a neuron with a small paradoxical alkalinization in response to $pMet\downarrow_1$—paradoxical because an isolated decrease in $[HCO_3^-]_o$ elicits a rise in pH_i and thus (because $[CO_2]_i \cong [CO_2]_o$) a rise in $[HCO_3^-]_i$—and a small acidification in response to MAc_2. The green trace also reports a paradoxical alkalinization during $pMet\downarrow_1$, followed by almost no change during MAc_2. Finally, the red trace again reveals a paradoxical alkalinization during $pMet\downarrow_1$, but then a marked acidification during MAc_2.

TABLE 6 State and behavior of 47 hippocampal neurons during exposure to isolated decrease of pH_o (pAc) and metabolic acidosis (MAc).

A, state:* pAc_1	27 neurons (57%) = resistant		20 neurons (43%) = sensitive		
B, state transition:† $pAc_1 \rightarrow MAc_2$	15 (32%) remain resistant [Q_I]	12 (25%) become sensitive [Q_{IV}]	3 (7%) become resistant [Q_{II}]	17 (36%) remain sensitive [Q_{III}]	
C, Behavior:‡ $pAc_1 \rightarrow MAc_2$*					Total
Adaptation	2 (4%)	0	3 (7%)	4 (9%)	9 (19%)
Consistency	10 (21%)	1 (2%)	0	2 (4%)	13 (28%)
Decompensation	3 (7%)	11 (23%)	0	11 (23%)	25 (53%)
D, State:† MAc_2 Resistant	18 (38%)		MAc_2 Sensitive	29 (62%)	

[a]State for pulse 1: resistant neurons are to the right of the vertical dashed blue line; sensitive neurons are to the left.
[b]State for pulse 2, resistant neurons are above the horizontal dashed blue line; sensitive neurons are below.
[c]Behaviors for pulse 1→2 transition: Adaptation (i.e., point is above the hourglass); Consistency (i.e., point is within the hourglass); Decompensation (i.e., point is below the hourglass). Q, quadrant; Q_I, quadrant I (neurons that are "resistant" during pAc_1, and remain resistant during MAc_2); Q_{II}, quadrant II (pAc_1 sensitive → MAc_2 resistant); Q_{III}, quadrant III (pAc_1 sensitive → pAc_2 sensitive); Q_{IV}, quadrant IV (pAc_1 resistant → MAc_2 sensitive).
Key points: The general trend is toward MAc_2 a sensitivity: Of 27 neurons with a resistant state during pAc_1 (row A), nearly half adopt a sensitive (12; Q_{IV}) state during MAc_2 (row A). Of 20 neurons with a sensitive state during pAc_1, the vast majority (17; Q_{III}) adopt a sensitive state during MAc_2.

Analyses #1–3

Figure 8B and Table 8 summarize the state and behavior for the full pMet↓-MAc dataset (n = 52; N = 17, $\mathcal{N}$ = 12). Because pH_o remains constant during $pMet\downarrow_1$, the ratio $\Delta pH_i/\Delta pH_o = \pm\infty$ (or undefined in the case of 0/0) for each neuron. Although it is impossible to position the vertical dashed blue line at ΔpH_i = 40% × pH_o, we elect to position it at $(\Delta pH_i)_{1/pMet\downarrow} = 0.08$, the value for the parent disturbance, $(\Delta pH_i)_{1/MAc}$.

The most striking characteristic of Figure 8B is that the vast majority of points fall to the right of the vertical dashed blue line, and all but five of 52 neurons lie in or below the hourglass. In other words, in a naïve neuron, pMet↓ produces only small pH_i decreases or even paradoxical pH_i increases, and the subsequent MAc_2 nearly always produces larger pH_i decreases that fulfill the criteria for decompensation behavior.

The blue point lies in Q_I (i.e., states are both $pMet\downarrow_1$ and MAc_2 resistant), well below the hourglass (i.e., behavior is decompensation), and lies to the right of the *y*-axis (i.e., $pMet\downarrow_1$ elicits a paradoxical alkalinization).

The green point, like the blue point, lies in Q_I (i.e., states are both $pMet\downarrow_1$ and MAc_2 resistant) and is below the hourglass (i.e., behavior is decompensation). It is not only to the right of the *y*-axis, it is just above the *x*-axis (i.e., $pMet\downarrow_1$ elicits a strong paradoxical alkalinization).

The red point lies in Q_{IV} (i.e., states are $pMet\downarrow_1$ resistant but MAc_2 sensitive), and well below the hourglass (i.e., behavior is decompensation).

The mean $d_\pm$ is −0.047 (Table 2, row 6), the most strongly negative value (consistent with decompensation) in the present study; this value is significantly different from zero ($P \cong 0.0001$).

ΔpH_i vs initial pH_i

Figure 8C reveals correlation strengths, taking all 52 points together, of "absent" for both $(\Delta pH_i)_{1/pMet\downarrow}$ vs $(pH_i)_1$, and $(\Delta pH_i)_{2/MAc}$ vs $(pH_i)_2$.

Frequency distributions

Figure 8D shows that the mean $(\Delta pH_i)_{1/pMet\downarrow}$ is substantially less than the mean for $(\Delta pH_i)_{2/MAc}$, and that the difference is highly significant.

Summary of pMet↓-MAc

$pMet\downarrow_1$ produces the smallest pH_i decrease of any first challenge in the present study, and often produces paradoxical pH_i increases.

MAc and then pMet↓

In this final experimental series, we reverse the order of pMet↓ and MAc from Figure 8, challenging the neurons first with MAc, and then with pMet↓.

Sample pH_i records

Figure 9A shows the remarkable pH_i responses of three HC neurons. The blue record is that of a neuron that acidifies slightly in response to MAc_1, hardly recovers upon withdrawal of the MAc_1 challenge, and then paradoxically alkalinizes during $pMet\downarrow_2$. The green trace shows a large acidification during MAc_1 but a modest, paradoxical alkalinization with $pMet\downarrow_2$. Finally, the red trace reports a small, paradoxical alkalinization in response to MAc_1, a paradoxical acidification upon removal of the MAc_1 challenge, and a large, paradoxical alkalinization during $pMet\downarrow_2$.

Analyses #1–3

Figure 9B and Table 9 summarize state and behavior for the full MAc-pMet↓ dataset (n = 61; N = 24, $\mathcal{N}$ = 9). As noted for $pMet\downarrow_1$ in Figure 8B, during $pMet\downarrow_2$ here in Figure 9B, $\Delta pH_i/\Delta pH_o = \pm\infty$ (or 0/0). Therefore, we elect to position the horizontal dashed blue line at $(\Delta pH_i)_{2/pMet\downarrow} = -0.08$, the value for the parent disturbance, $(\Delta pH_i)_{2/MAc}$.

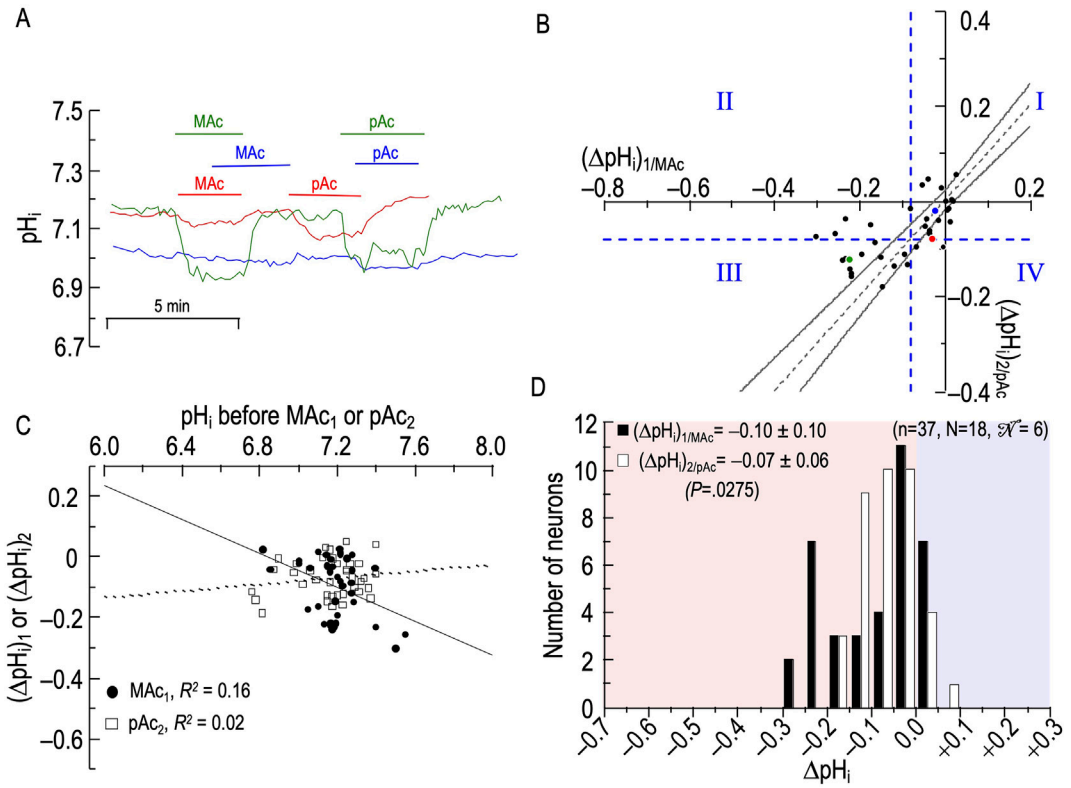

FIGURE 7
Effect of metabolic acidosis (MAc) followed by pure acidosis (pAc) on the pH_i of rat hippocampal neurons **(A)**, examples of the pH_i responses in three hippocampal neurons to an exposure to MAc (solution 3, Table 1), and then to pAc (solution 5, Table 1). Unless otherwise indicated, the bath solution was standard CO_2/HCO_3^- (solution 2, Table 1). **(B)**, relationship between the ΔpH_i during exposure to MAc—that is, $(\Delta pH_i)_{1/MAc}$—and ΔpH_i during exposure to pAc—that is, $(\Delta pH_i)_{2/pAc}$. The horizontal and vertical dashed blue lines are the resistant-sensitive demarcations that define quadrants I–IV and "pH_i states" (see Figure 3). The blue dot that represents the blue neuron in panel A is in Q_I (i.e., neuron is both MAc_1 and pAc_2 resistant). The green dot is in Q_{III} (i.e., green neuron in panel A is both MAc_1 and pAc_2 sensitive). Because the red dot is on the horizontal dashed blue line, it is in Q_I (i.e., red neuron in panel A is both MAc_1 and pAc_2 resistant). The dashed gray line is the line of identity; the gray hourglass represents the confidence interval and defines "pH_i behavior" (see Figure 3). Because the blue point lies within the hourglass, the behavior of the blue neuron is consistency. The green point lies above the upper asymptote of the hourglass; the behavior is adaptation. The red neuron lies below the lower asymptote of the hourglass; the behavior is decompensation. **(C)**, dependence of $(\Delta pH_i)_1$ (black circles) on the initial pH_i before MAc_1, which we refer to as $(\Delta pH_i)_{1/MAc}$, or dependence of $(\Delta pH_i)_2$ (white squares) on the initial pH_i before and pAc_2, which we refer to as $(\Delta pH_i)_{2/pAc}$. The solid and dashed lines represent the linear regressions for MAc_1 and pAc_2, respectively. **(D)**, frequency distribution of $(\Delta pH_i)_{1/MAc}$ (black bars) and $(\Delta pH_i)_{2/pAc}$ (white bars) with a pH_i bin width of 0.05 pH units. In the upper left, we report means ± standard deviation as well as the *p*-value (paired t-test, two-tails). n, number of neurons; N, number of cover slips; $\mathcal{N}$, number of animals/cultures.

The most striking aspects of Figure 9B are that few neurons are below the *x*-axis, and none are below either the horizontal dashed blue line or the hourglass. Thus, MAc pretreatment produces a dramatic alkaline-shift of the pH_i response to $pMet\downarrow_2$ during the second challenge. In fact, 87% of the neurons exhibit a frank alkalinization.

The blue point lies in Q_I (i.e., states are both MAc_1 and $pMet\downarrow_2$ resistant), above the hourglass (i.e., behavior is adaptation), and above the *x*-axis (i.e., $pMet\downarrow_2$ elicits a paradoxical alkalinization).

The green point lies in Q_{II} (i.e., states are MAc_1 sensitive but $pMet\downarrow_2$ resistant), above the hourglass (i.e., behavior is adaptation), and above the *x*-axis (i.e., $pMet\downarrow_2$ elicits a paradoxical alkalinization).

The red point lies on the Q_I (i.e., states are both MAc_1 and $pMet\downarrow_2$ resistant), above the hourglass (i.e., behavior is adaptation), as well as to the right of the *y*-axis and above the *x*-axis (i.e., both MAc_1 and $pMet\downarrow_2$ elicit paradoxical alkalinizations).

The mean $d_{\pm}$ is +0.094 (Table 2, row 7), the most strongly positive value in the present study; this value is significantly different from zero ($p \cong 2.3\times10^{-15}$), consistent with adaptation.

ΔpH_i vs initial pH_i

Figure 9C reveals correlation strengths, taking all 61 points together, of "absent" for $(\Delta pH_i)_{1/MAc}$ vs $(pH_i)_1$, and "weak" $(\Delta pH_i)_{2/pMet\downarrow}$ vs $(pH_i)_2$.

Frequency distributions

The subset of neurons summarized Figure 9D has a mean $(\Delta pH_i)_{1/MAc}$ of −0.07, less than the global value of −0.11 across the entire study (see Figure 1). However, far more striking is the mean $(\Delta pH_i)_{2/pMet\downarrow}$, which is shifted far to the right, at a positive value of +0.06. The difference is highly significant.

TABLE 7 State and behavior of 37 hippocampal neurons behavior during metabolic acidosis (MAc) and to an isolated decrease of pH_o (pAc) exposure.

A, state:* MAc_1	20 neurons (54%) = resistant		17 neurons (46%) = sensitive		
B, state transition:† $MAc_1 \rightarrow pAc_2$	18 (49%) remain resistant [Q_I]	2 (5%) become sensitive [Q_{IV}]	4 (11%) become resistant [Q_{II}]	13 (35%) remain sensitive [Q_{III}]	
C, Behavior:‡ $MAc_1 \rightarrow pAc_2$*					Total
Adaptation	4 (11%)	0	4 (11%)	8 (22%)	16 (43%)
Consistency	5 (14%)	0	0	3 (8%)	8 (22%)
Decompensation	9 (24%)	2 (5%)	0	2 (5%)	13 (35%)
D, State:† pAc_2 Resistant	22 (60%)		pAc_2 Sensitive	15 (40%)	

[a]State for pulse 1: resistant neurons are to the right of the vertical dashed blue line; sensitive neurons are to the left.
[b]State for pulse 2, resistant neurons are above the horizontal dashed blue line; sensitive neurons are below.
[c]Behaviors for pulse 1→2 transition: Adaptation (i.e., point is above the hourglass); Consistency (i.e., point is within the hourglass); Decompensation (i.e., point is below the hourglass). Q, quadrant; Q_I, quadrant I (neurons that are resistant during MAc_1, and remain "resistant" during MAc_2); Q_{II}, quadrant II (MAc_1 sensitive → pAc_2 resistant); Q_{III}, quadrant III (MAc_1 sensitive → pAc_2 sensitive); Q_{IV}, quadrant IV (MAc_1 resistant → pAc_2 sensitive).
Key points: The neurons tend to maintain their "state" between MAc_1 (row A) and pAc_2 (row B). Thus, 18 of 20 neurons that were MAc_1 resistant also fulfill the MAc, criteria for resistance during pAc_2 (Q_I), and 13 of 17 neurons that were MAc_1 sensitive also fulfill the MAc, criteria for sensitivity in pAc_2 (Q_{III}). We suggest that this MAc_1–pAc_2 comparison is valid because our global $(\Delta pH_i)_{1/MAc}$, of −0.11 in Figure 1 is very similar to the $(\Delta pH_i)_{1/pAc}$ of −0.10 in the pAc-MAc, protocol (Figure 6D). Although nearly 85% of the neurons lie in Q_I, or Q_{III}, only a small fraction (22%) of MAc-pAc neurons fulfill the MAc-MAc, criteria for consistency.

Summary of MAc-pMet↓

Pretreatment with MAc causes 87% of neurons to alkalinize paradoxically in response to $pMet\downarrow_2$.

Discussion

Historical background and comparisons

Previous work from this laboratory has shown that, in response to MAc, the cytosol of hippocampal neurons acidifies to varying extents, with some neurons undergoing relatively small pH_i decreases and being described as "resistant" (Bouyer et al., 2004). In a subsequent study of ten different cell types, including co-cultured mouse HC neurons and astrocytes, Salameh et al. (2014) numerically defined "MAc resistant" and "MAc sensitive". Salameh et al. (2014) also introduced and defined the terms "adaptation," "consistency," and "decompensation" to describe the change in MAc-induced ΔpH_i values between the first and second of two MAc challenges. Salameh et al. (2017) later established that the acceleration of the Cl-HCO_3 exchanger AE3 (a potent acid loader) plays a central role in determining the rate and extent of the MAc-induced acidification of HC neurons. Thus, we expect that the fall in $[HCO_3^-]_o$ per se—one component of MAc—to accelerate AE3 and thereby contribute to the MAc-induced fall in pH_i. However, we do not know whether the fall in $[HCO_3^-]_o$, by other mechanisms (e.g., effects on other transporters or regulatory processes), contributes to the fall in pH_i. Nor do we know whether the concomitant fall in pH_o per se—the other component of MAc—also contributes to the MAc-induced fall in pH_i.

Understanding the mechanism of action of MAc is crucial for two reasons. First, several diseases can cause MAc. These include sepsis, diabetic ketoacidosis, ischemia/hypoxia (causing lactic acidosis), kidney disease (causing renal tubular acidosis), and gastrointestinal diseases (causing severe diarrhea). Second, MAc can negatively affect various organ systems, even to the extent of being life-threatening (Lim, 2007; Gennari and Weise, 2008; Raphael et al., 2016; Raphael, 2018).

Of the 235 naïve neurons exposed to MAc in the present study, ~62% were MAc sensitive and ~38% were resistant. This distribution is similar to the one reported by Salameh et al. (2014) but differs from our first study, in which we reported that the majority of hippocampal neurons were resistant (Bouyer et al., 2004). Part of this difference is due to the resistant/sensitive criteria later established by Salameh et al. (2014), and the rest presumably arises from the small number of neurons (14 neurons) in that first study, compared to 25 in the work by Salameh et al. (2014), and 235 in the present study.

Zhou et al. (2005) previously reported the effects of select OOE solutions on steady-state pH_i in rabbit proximal tubules. The present study is the first on vertebrate cells to report pH_i time courses during the application and removal of OOE solutions. Following up on previous work on the effects of MAc and MAc-MAc on neurons and other cells by Salameh et al. (2014), our major goal in the present study was to use OOE technology as a tool to dissect the effects of MAc into two of its major component parts (1) an isolated decrease in pH_o (i.e., pAc): and (2) an isolated decrease in $[HCO_3^-]_o$ (i.e., pMet↓).

Effects of acid-base challenges on $[CO_3^=]_o$

As noted by Zhao et al. (2003) and Bouyer et al. (2024), the approach for creating OOE solutions does not permit independent

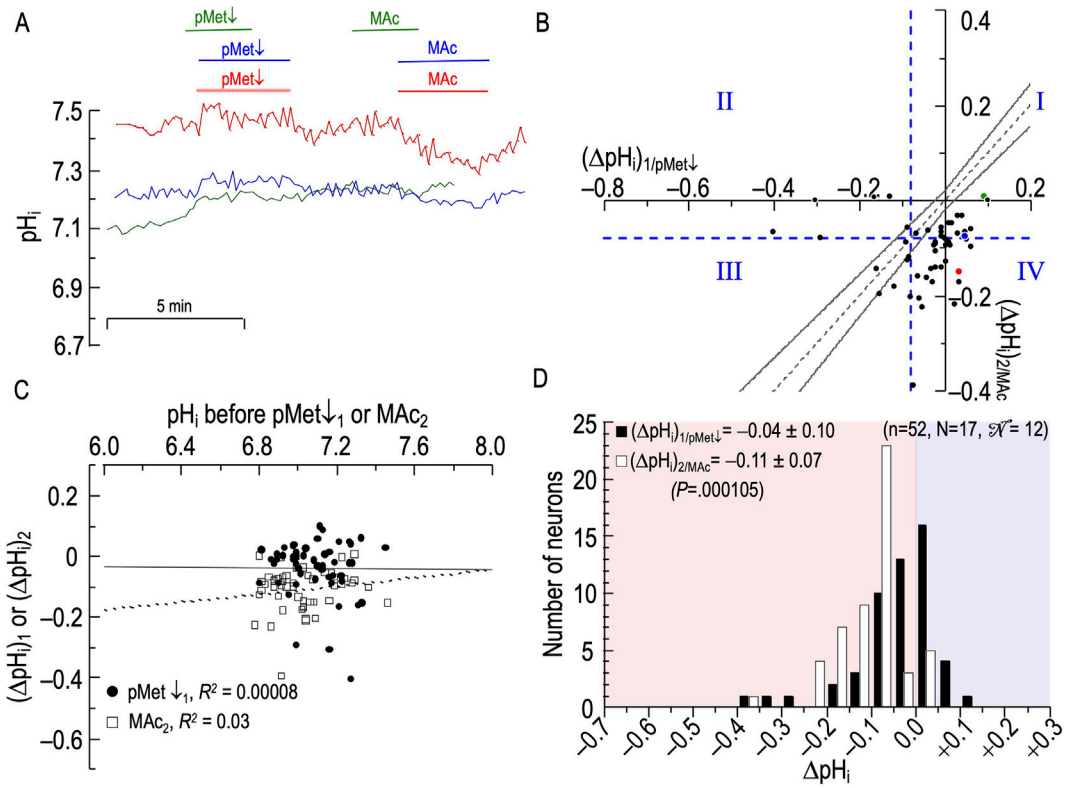

FIGURE 8
Effect of an isolated decrease of $[HCO_3^-]_o$ (pMet↓) followed by metabolic acidosis (MAc) on the pH_i of rat hippocampal neurons **(A)**, examples of the pH_i responses in three hippocampal neurons to an exposure to pMet↓ (solution 6, Table 1), and then to MAc (solution 3, Table 1). Unless otherwise indicated, the bath solution was standard CO_2/HCO_3^- (solution 2, Table 1). **(B)**, relationship between the ΔpH_i during exposure to pMet↓—that is, $(\Delta pH_i)_{1/pMet\downarrow}$—and ΔpH_i during exposure to MAc—that is, $(\Delta pH_i)_{2/MAc}$. The horizontal and vertical dashed blue lines are the resistant-sensitive demarcations that define quadrants I–IV and "pH_i states" (see Figure 3). The blue dot that represents the blue neuron in panel **(A)** is in Q_I (i.e., neuron is both pMet↓ and MAc_2 resistant). The green dot also is in Q_I (i.e., green neuron in panel **(A)** is both pMet↓ and MAc_2 resistant). The red dot is in Q_{IV} (i.e., red neuron in panel **(A)** is pMet$\downarrow_1$ resistant but MAc_2 sensitive). Note that, for all three neurons, $(\Delta pH_i)_{1/pMet\downarrow}$ is paradoxically positive. Additionally, for the green neuron, $(\Delta pH_i)_{2/MAc}$ is positive. The dashed gray line is the line of identity; the gray hourglass represents the confidence interval and defines "pH_i behavior" (see Figure 3). Because the blue, green, and red points all lie below the lower asymptote of the hourglass, the behavior of the three corresponding neurons is decompensation. **(C)**, dependence of $(\Delta pH_i)_1$ (black circles) on the initial pH_i before pMet↓, which we refer to as $(\Delta pH_i)_{1/pMet\downarrow}$, or dependence of $(\Delta pH_i)_2$ (white squares) on the initial pH_i before and MAc_2, which we refer to as $(\Delta pH_i)_{2/MAc}$. The solid and dashed lines represent the linear regressions for pMet$\downarrow_1$ and MAc_2, respectively. **(D)**, frequency distribution of $(\Delta pH_i)_{1/pMet\downarrow}$ (black bars) and $(\Delta pH_i)_{2/MAc}$ (white bars) with a pH_i bin width of 0.05 pH units. In the upper left, we report means ± standard deviation as well as the *p*-value (paired t-test, two-tails). n, number of neurons; N, number of cover slips; $\mathcal{N}$, number of animals/cultures.

control over $CO_3^=$ or $NaCO_3^-$. These solutes are important because, as suggested earlier (Boron and Boulpaep, 1983; Boron and Russell, 1983; Boron, 1985; Boron and Knakal, 1989; 1992), a combination of electrophysiological and modeling approaches now shows that either $CO_3^=$ or the $NaCO_3^-$ ion pair is the actual substrate of both the electrogenic Na/HCO_3 cotransporter NBCe1 and the Na^+-driven $Cl\text{-}HCO_3$ exchanger NDCBE (Lee et al., 2023). Because both transporters play important roles in pH_i regulation of both neurons and astrocytes, it is instructive to consider how our experimental challenges impact $[CO_3^=]_o$:

- During MAc in our experiments, $[HCO_3^-]_o$ falls from 22 mM to ~14 mM, which is ~63% of the initial value. Simultaneously, pH_o falls from 7.40 to 7.20, which means that $[H^+]_o$ rises by a factor of 1/(~63%) or ~58%. The rise in $[H^+]_o$ produces a reciprocal fall in $[CO_3^=]_o$. Thus, this combination of $[HCO_3^-]_o$ and pH_o changes in MAc causes $[CO_3^=]_o$ to fall to about 63 % × 63 % or ~40% of its initial value.
- During pAc, where $[CO_2]_o$ and $[HCO_3^-]_o$ are fixed, $[H^+]_o$ rises by ~58% (i.e., corresponding to the same 0.2 pH_o decrease as in MAc), which causes a reciprocal decrease in $[CO_3^=]_o$, which falls to ~63% of its initial value.
- During pMet↓, where $[CO_2]_o$ and $[H^+]_o$ are fixed, $[HCO_3^-]_o$ falls to ~63% of its initial value (as in MAc), which causes $[CO_3^=]_o$ to fall to ~63% of its initial value.

In summary, pAc and pMet↓ each produce 37% decreases in $[CO_3^=]_o$, and also $[NaCO_3^-]_o$, whereas MAc produces a 60% decrease.

Comparison of effects of MAc vs those of pAc + pMet↓

In this section, we ask whether the effects of MAc are merely the sum of the individual effects of pAc and pMet↓. Based on our discussion of how each challenge affects $[CO_3^=]_o$, we expect

10.3389/fphys.2024.1434359

TABLE 8 State and behavior of 52 hippocampal neurons behavior during an isolated decrease of $[HCO_3^-]_o$ (pMet↓) and MAc exposure.

A, state:* pMet↓$_1$	40 neurons (77%) = resistant		12 neurons (23%) = sensitive		
B, state transition:† pMet↓$_1$ → MAc$_2$	16 (31%) remain resistant [Q_I]	24 (46%) become sensitive [Q_{IV}]	6 (11.5%) become resistant [Q_{II}]	6 (11.5%) remain sensitive [Q_{III}]	
C, Behavior:‡ pMet↓$_1$ → MAc$_2$*					Total
Adaptation	1 (2%)	0	5 (9%)	0	6 (11%)
Consistency	1 (2%)	0	1 (2%)	2 (4%)	4 (8%)
Decompensation	14 (27%)	24 (46%)	0	4 (8%)	42 (81%)
D, State:† MAc$_2$ Resistant	22 (42%)		MAc$_2$ Sensitive	30 (58%)	

*State for pulse 1: resistant neurons are to the right of the vertical dashed blue line; sensitive neurons are to the left.
†State for pulse 2, resistant neurons are above the horizontal dashed blue line; sensitive neurons are below.
‡Behaviors for pulse 1→2 transition: Adaptation (i.e., point is above the hourglass); Consistency (i.e., point is within the hourglass); Decompensation (i.e., point is below the hourglass). Q, quadrant; Q_I, quadrant I (neurons that are "resistant" during pMet↓$_1$, and remain resistant during MAc$_2$); Q_{II}, quadrant II (pMet↓$_1$ sensitive → MAc$_2$ resistant); Q_{III}, quadrant III (pMet↓$_1$ sensitive → MAc$_2$ sensitive); Q_{IV}, quadrant IV (pMet↓$_1$ resistant → MAc$_2$ sensitive).
Key points: Most neurons (40 of 52) are resistant during pMet↓$_1$ by MAc, criteria (row A). Of these, most (24 of 40) are sensitive during MAc$_2$ (row B). Of the few neurons (12 of 52) that are pMet↓$_1$ sensitive, equal numbers are resistant vs sensitive during MAc$_2$. The rightmost column of the table reveals that >80% of the neurons fulfill the criteria for decompensation.

the decrease in $[CO_3^=]_o$ during MAc (~60%) to be modestly less than the sum of the decreases during pAc (~37%) and pMet↓ (~37%).[9]

(1) Effects on $(\Delta pH_i)_1$: MAc$_1$ vs pAc$_1$ + pMet↓$_1$

The simplest question addresses "state": is the effect of MAc on ΔpH_i in a naïve neuron merely the sum of the acidosis (i.e., pAc) and the decrease in $[HCO_3^-]_o$ (i.e., pMet↓)? To address this query, we compare MAc$_1$ (Figure 3) vs pAc$_1$ (Figure 6) and pMet↓$_1$ (Figure 8). The answer seems to be approximately "yes." If we sum the ΔpH_i for the first challenge in each of these figures (compare Figure 3D vs Figures 6D vs; Figure 8D), we have a near-exact match:[10]

$$\underbrace{(\Delta pH_i)_{1/MAc}}_{\underbrace{-0.14}_{Fig\,3D}} \overset{?}{=} \underbrace{(\Delta pH_i)_{1/pAc}}_{\underbrace{-0.10}_{Fig\,6D}} + \underbrace{(\Delta pH_i)_{1/pMet\downarrow}}_{\underbrace{-0.04}_{Fig\,8D}} \cong \underbrace{-0.14}_{} \quad (3)$$

If instead, we use the global $(\Delta pH_i)_{1/MAc}$ from Figure 1, we observe only a modest difference

$$\underbrace{(\Delta pH_i)_{1/MAc}}_{\underbrace{-0.11}_{Fig\,1}} \overset{?}{=} \underbrace{(\Delta pH_i)_{1/pAc}}_{\underbrace{-0.10}_{Fig\,6D}} + \underbrace{(\Delta pH_i)_{1/pMet\downarrow}}_{\underbrace{-0.04}_{Fig\,8D}} \cong \underbrace{-0.14}_{} \quad (4)$$

One note of caution is that, because we did not set out to perform a systematic comparison of MAc vs pAc and pMet↓, we did not routinely perform all three protocols on the same day on naïve neurons from the same cultures. Nevertheless, we are comparing data from a large number of neurons, coverslips, and cultures across a large portion of the present study.

A second note of caution is that, as noted above under "Effects of acid-base challenges on $[CO_3^=]_o$", the sum $(\Delta[CO_3^=]_o)_{1/pAc} + (\Delta[CO_3^=]_o)_{1/pMet\downarrow}$ is a somewhat larger negative number than $(\Delta[CO_3^=]_o)_{1/MAc}$:

$$\underbrace{\left(\Delta[CO_3^=]_i\right)_{1/MAc}}_{\underbrace{\downarrow 60\%}_{Fig\,3}} \overset{?}{=} \underbrace{\left(\Delta[CO_3^=]_i\right)_{1/pAc}}_{\underbrace{\downarrow 37\%}_{Fig\,6}} + \underbrace{\left(\Delta[CO_3^=]_i\right)_{1/pMet\downarrow}}_{\underbrace{\downarrow 37\%}_{Fig\,8}} \quad (5)$$
$$< \underbrace{\quad\quad}_{\downarrow 74\%}$$

This inequality could contribute to the any imbalance in Equation 3 and Equation 4. Moreover, the three acid-base challenges presumably also lead to different changes in various cytosolic parameters (see Bouyer et al., 2024) that could contribute to ΔpH_i in ways that are not algebraically additive. For example, in all three disturbances, $[CO_2]_o$ is fixed, so that the induced changes in pH_i translate directly to changes in $[HCO_3^-]_i$ and $[CO_3^=]_i$, which could in turn have nonlinear effects on the kinetics of transporters.

Our conclusion from this first analysis is that for naïve neurons—cells experiencing a challenge for the first time—the whole (MAc$_1$) is very nearly the sum of the parts (pAc$_1$ + pMet↓$_1$). We address this additivity in Bouyer et al. (2024).

(2) Effects of MAc$_1$ on $(\Delta pH_i)_{2/MAc}$ vs $(\Delta pH_i)_{2/pAc}$ + $(\Delta pH_i)_{2/pMet\downarrow}$

Question '2' is similar to '1', but addresses "behavior" across twin-pulse challenges. Here we ask whether the effect of MAc$_1$ on MAc$_2$ (Figure 3B) is the sum of the effects of MAc$_1$ on pAc$_2$ (Figure 7B) and MAc$_1$ on pMet↓$_2$ (Figure 9B). First, examining the ΔpH_i values:

9 In the present study, we examine only a subset of properties related to acid-base physiology. One could address our question to a far greater range of pH_i-related properties, let alone those related to a host of other areas such as the homeostasis of other ions and electrophysiological activity.

10 In this and subsequent equations, the bolded subscripts indicate the parameters on which we are focusing.

10.3389/fphys.2024.1434359

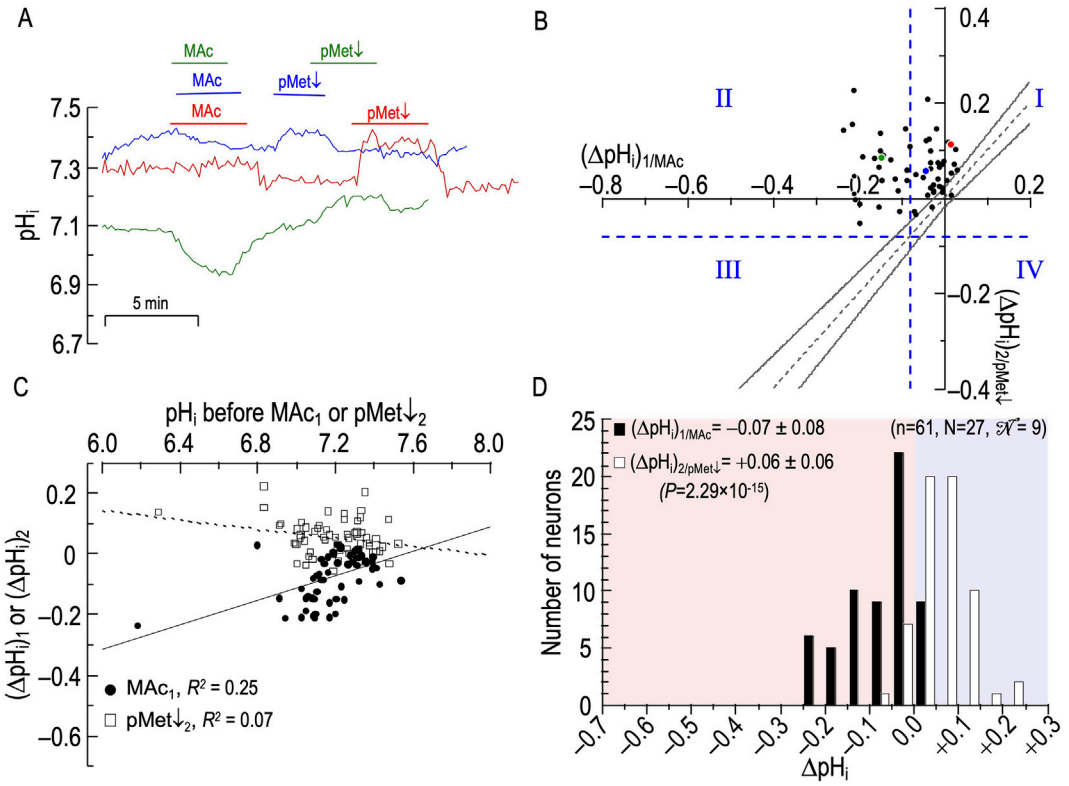

FIGURE 9
Effect of metabolic acidosis (MAc) followed by pure metabolic/down (pMet↓) on the pH_i of rat hippocampal neurons **(A)**, examples of the pH_i responses in three hippocampal neurons to an exposure to MAc (solution 3, Table 1), and then to pMet↓ (solution 6, Table 1). Unless otherwise indicated, the bath solution was standard CO_2/HCO_3^- (solution 2, Table 1). **(B)**, relationship between the ΔpH_i during exposure to MAc—that is, $(\Delta pH_i)_{1/MAc}$—and ΔpH_i during exposure to pMet↓—that is, $(\Delta pH_i)_{2/pMet\downarrow}$. The horizontal and vertical dashed blue lines are the resistant-sensitive demarcations that define quadrants I–IV and "pH_i states" (see Figure 3). The blue dot that represents the blue neuron in panel **(A)** is in Q_I (i.e., neuron is both pMet↓ and MAc_2 resistant). The green dot is in Q_{II} (i.e., green neuron in panel **(A)** is MAc_1 sensitive but $pMet\downarrow_2$ resistant). The red dot is in Q_I (i.e., red neuron in panel **(A)** is both MAc_1 $pMet\downarrow_2$ resistant). Note that, for all three neurons, $(\Delta pH_i)_{2/pMet\downarrow}$ is paradoxically positive. Additionally, for the red neuron, $(\Delta pH_i)_{1/MAc}$ is positive. The dashed gray line is the line of identity; the gray hourglass represents the confidence interval and defines "pH_i behavior" (see Figure 3). Because the blue, green, and red points are all above the upper asymptote of the hourglass, the behavior is adaptation. **(C)**, dependence of $(\Delta pH_i)_1$ (black circles) on the initial pH_i before MAc_1, which we refer to as $(\Delta pH_i)_{1/MAc}$, or dependence of $(\Delta pH_i)_2$ (white squares) on the initial pH_i before and $pMet\downarrow_2$, which we refer to as $(\Delta pH_i)_{2/pMet\downarrow}$. The solid and dashed lines represent the linear regressions for Ac_1 and MAc_2, respectively. **(D)**, frequency distribution of $(\Delta pH_i)_{1/MAc}$ (black bars) and $(\Delta pH_i)_{2/pMet\downarrow}$ (white bars) with a pH_i bin width of 0.05 pH units. In the upper left, we report means ± standard deviation as well as the *p*-value (paired t-test, two-tails). n, number of neurons; N, number of cover slips; $\mathcal{N}$, number of animals/cultures.

$$\underbrace{(\Delta pH_i)_{1/MAc-2/MAc}}_{-0.11\ (Fig\ 3D)} \overset{?}{=} \underbrace{(\Delta pH_i)_{1/MAc-2/pAc}}_{-0.07\ (Fig\ 7D)} + \underbrace{(\Delta pH_i)_{1/MAc-2/pMet\downarrow}}_{+0.06\ (Fig\ 9D)} \quad (6)$$

$$\underbrace{(d_\pm)_{1/MAc-2/MAc}}_{+0.024\ (Fig\ 3B)} \overset{?}{=} \underbrace{(d_\pm)_{1/MAc-2/pAc}}_{+0.020\ (Fig\ 7B)} + \underbrace{(d_\pm)_{1/MAc-2/pMet\downarrow}}_{+0.094\ (Fig\ 9B)} \quad (7)$$

In Equation 6, the three (ΔpH_i) values refer to the mean $(\Delta pH_i)_2$ in protocols in which the first challenge was always MAc_1, but the second challenges were MAc_2 on the left vs pAc_2 and $pMet\downarrow_2$ on the right. Thus, observing $(\Delta pH_i)_2$, we see that the effects of MAc_1 on $(\Delta pH_i)_{2/pAc}$ and $(\Delta pH_i)_{2/pMet\downarrow}$ very nearly cancel one another (i.e., −0.01), as they sum to a value that is markedly smaller than the effect of MAc_1 on $(\Delta pH_i)_{2/MAc}$ (i.e., −0.11).

Viewed from the perspective of $d_\pm$, in the MAc-MAc protocol, $d_\pm$ is +0.024 (see Table 2), compared to a $d_\pm$ of +0.020 in the MAc-pAc protocol and a $d_\pm$ of +0.094 in the MAc-pMet↓ protocol. Thus, for these three protocols that have in common that the first challenge is MAc, we ask in equation form:

In other words, with MAc_1 as the first challenge and MAc_2 as the second, we see a modest adaptive effect (+0.024), whereas the two component second challenges—pAc_2 (modest adaptive effect) and $pMet\downarrow_2$ (strong adaptive effect)—produce effects that sum to an extremely strong adaptive effect (+0.114). Clearly, the whole is much less than the sum of the parts.

From this third analysis, whether we examine ΔpH_i or $d_\pm$, we conclude that—when the first challenge is MAc_1—the whole (MAc_2) is very different from sum of the parts (pAc_2 + $pMet\downarrow_2$).

Similar to what we proposed above regarding question '2', we suggest that—following MAc_1—the machinery triggered by pAc_2 and $pMet\downarrow_2$ intersect in such a way that, in combination but not alone, the two produce a modest, net adaptation behavior. In other

TABLE 9 State and behavior of 61 hippocampal neurons behavior during exposure to MAc and an isolated decrease of $[HCO_3^-]_o$ (pMet↓).

A, state:* MAc_1	35 neurons (57%) = resistant		26 neurons (43%) = sensitive		
B, state transition:† $MAc_1 \rightarrow pMet\downarrow_2$	35 (57%) remain resistant [Q_I]	0 (0%) become sensitive [Q_{IV}]	26 (43%) become resistant [Q_{II}]	0 remain sensitive [Q_{III}]	
C, Behavior:‡ $MAc_1 \rightarrow pMet\downarrow_2$*					Total
Adaptation	30 (49%)	0	26 (43%)	0	56 (92%)
Consistency	5 (8%)	0	0	0	5 (8%)
Decompensation	0	0	0	0	0
D, State:† $pMet\downarrow_2$ Resistant	61 (100%)		$pMet\downarrow_2$ Sensitive	0	

*State for pulse 1: resistant neurons are to the right of the vertical dashed blue line; sensitive neurons are to the left.

†State for pulse 2, resistant neurons are above the horizontal dashed blue line; sensitive neurons are below.

‡Behaviors for pulse 1→2 transition: Adaptation (i.e., point is above the hourglass); Consistency (i.e., point is within the hourglass); Decompensation (i.e., point is below the hourglass). Q, quadrant; Q_I, quadrant I (neurons that are resistant during MAc_1, and remain "resistant" during $pMet\downarrow_2$); Q_{II}, quadrant II (MAc_1 sensitive → $pMet\downarrow_2$ resistant); Q_{III}, quadrant III (MAc_1 sensitive → $pMet\downarrow_2$ sensitive); Q_{IV}, quadrant IV (MAc_1 resistant → $pMet\downarrow_2$ sensitive).

Key points: The population of HC, neurons used in these experiments has a greater fraction of MAc_1-resistant cells (35 of 61 = 57% to the right of the vertical dashed blue line) than in other parts of the present paper. All of the neurons that are resistant during MAc_1 remain so during $pMet\downarrow_2$, and all of the neurons that are sensitive during MAc_1 shift to fulfill the MAc_2 criteria for resistance during $pMet\downarrow_2$—that is, all the neurons are resistant during $pMet\downarrow_2$. 92% of the neurons fulfill the criteria for adaptation. Although these data are not listed in this table, MAc_1-resistant neurons had a somewhat greater probability (32 of 35 = 91%) undergoing a paradoxical alkalinization during $pMet\downarrow_2$ than did MAc_1-sensitive neurons (21 of 26 = 81%).

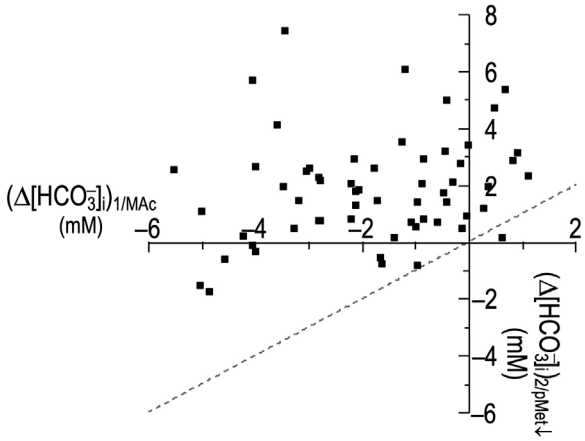

FIGURE 10
Effect of the MAc-pMet↓ protocol on computed $[HCO_3^-]_i$. Here we plot $[HCO_3^-]_i$ values that we computed from the same primary pH_i data that yielded the ΔpH_i data in Figure 9B, with the assumption that $[CO_2]_o = [CO_2]_o$. On the abscissa is the $\Delta[HCO_3^-]_i$ during MAc_1, and on the ordinate, the $\Delta[HCO_3^-]_i$ during $pMet\downarrow_2$. The dashed gray line represents the line of identity. Note that the pH-driven concepts of resistant/sensitive (which gave us the vertical and horizontal dashed blue lines in Figure 3B through Figure 9B) and the hourglass have no meaning in the plot we show here because the $\Delta[HCO_3^-]_i$ depends not just on ΔpH_i but also on the pH_i just before the imposition of MAc_1.

words, the $\downarrow(pH_o)_2$ and $\downarrow([HCO_3^-]_o)_2$ signals must be coincident in order to produce the physiological effect of MAc_2. We address the issue of coincidence in Bouyer et al. (2024).

(3) Effects on $(\Delta pH_i)_{2/MAc}$: Ac_1 vs pAc_1

It is instructive to compare the effects of Ac_1 vs pAc_1 on $(\Delta pH_i)_{2/MAc}$ because Ac_1 and pAc_1 (from the perspective of pH_o) differ only in the absence vs presence of CO_2/HCO_3^-. In the Ac-MAc protocol (see Figure 4D), $(\Delta pH_i)_{2/MAc}$ is −0.09, whereas in the pAc-MAc protocol (see Figure 6D), $(\Delta pH_i)_{2/MAc}$ is −0.13. Although these means are not significantly different (p = .0982), the trend is for acidosis in the presence of CO_2/HCO_3^- to produce a more negative $(\Delta pH_i)_{2/MAc}$, consistent with a trend towards greater decompensation.

We see an analogous but stronger pattern when we compare $d_\pm$ values (see Table 2). The $d_\pm$ of +0.015 for Ac-MAc (see also Figure 4B) is exactly opposite the $d_\pm$ of −0.015 for pAc-MAc (see also Figure 6B). Again, although the difference in mean $d_\pm$ values is not statistically significant (p = .0919), the trend is toward greater decompensation when the acidosis in the first challenge, occurs in the presence of CO_2/HCO_3^-.

Paradoxical effects of pMet↓

The effects of pMet↓ are truly unique. In the naïve neurons of Figure 8A and B, 19 of 52 (36%) of neurons exhibit a paradoxical pH_i increase—a positive $(\Delta pH_i)_{1/pMet\downarrow}$.

Even more striking is the MAc-pMet↓ protocol (see Figures 9A, B), where MAc_1 pretreatment causes the response to $pMet\downarrow_2$ to be a frank pH_i increase in 53 of 61 (~87%) of the neurons. In Figure 10, we use the pH_i data from Figure 9B to produce a plot of $(\Delta[HCO_3^-]_i)_{1/MAc}$ vs $(\Delta[HCO_3^-]_i)_{2/pMet\downarrow}$. All but one of the points lie above the LOI; that is, in 60 of 61 neurons, $(\Delta[HCO_3^-]_i)_{2/pMet\downarrow} > (\Delta[HCO_3^-]_i)_{1/MAc}$. Moreover, 53 of 61 neurons (the same 53 as in Figure 9B) lie above the x-axis. In other words, in these 87% of neurons, $pMet\downarrow_2$ (i.e., reducing $[HCO_3^-]_o$ from 22 to ~14 mM) causes $[HCO_3^-]_i$ to rise. This effect is analogous to putting 61 glasses of room-temperature water into a (functioning) refrigerator and removing the glasses 5 min later, only to find that the water temperature has paradoxically risen in 53 of 61 glasses (!).

As we speculate in Bouyer et al. (2024), the paradoxical pH_i increase during $pMet\downarrow_1$ in many naïve neurons in Figures 8A, B—a "state"—likely reflects a novel response to the decrease in $[HCO_3^-]_o$ *per se*, perhaps mediated by receptor protein tyrosine phosphatases γ

(RPTPγ) and/or ζ (RPTPζ), both of which are expressed in mouse HC neurons (Taki et al., 2024).

The paradoxical pH_i increase during pMet↓$_2$ of the twin MAc-pMet↓ challenge in Figures 9A, B—a "behavior"—could reflect the actions of intracellular and extracellular acid-base sensors (including the RPTPs) during MAc_1, as well as the RPTPs during pMet↓$_2$. It may be that, during a MAc-MAc protocol, the collection of all intra- and extracellular sensors acting during MAc_1 make the neuron better able to withstand a subsequent MAc_2. However, when pMet↓$_2$ replaces MAc_2, the lone immediate challenge to the now-prepared neuron is a decrease in $[HCO_3^-]_o$. The unbalanced response of the hypothetical receptor to low $[HCO_3^-]_o$ could be a massive stimulation of acid extruders (vs acid loaders), resulting in the strong and nearly uniform paradoxical pH_i increase.

Summary and conclusions

- **Sensing:** Rat HC neurons can separately sense and respond to ↓(pH_o) and ↓($[HCO_3^-]_o$).
- **State:** In naïve HC neurons, the separate ↓(pH_o) and ↓($[HCO_3^-]_o$) signals summate to yield the same ΔpH_i as the simultaneous ↓(pH_o)/↓($[HCO_3^-]_o$) signals.
- **Behavior:** When HC neurons cross the boundary between two acid-base challenges, the ΔpH_i or $d_{\pm}$ response is a complex event that requires coincident pAc and pMet↓ signals.

Data availability statement

The raw data supporting the conclusions of this article will be made available by the authors, without undue reservation.

Ethics statement

The animal study was approved by J. Michael Oakes/Senior Vice President for Research, Office of Research and Technology Management. The study was conducted in accordance with the local legislation and institutional requirements.

Author contributions

PB: Investigation, Writing–review and editing, Writing–original draft, Validation, Project administration, Methodology, Formal Analysis, Data curation, Conceptualization. AS: Validation, Writing–review and editing, Formal Analysis, Data curation. YZ: Validation, Writing–review and editing, Methodology, Formal Analysis, Data curation. TK: Writing–review and editing, Methodology, Data curation, Formal Analysis. WB: Writing–review and editing, Writing–original draft, Validation, Supervision, Resources, Project administration, Methodology, Funding acquisition, Formal Analysis, Data curation, Conceptualization.

Funding

The author(s) declare that financial support was received for the research, authorship, and/or publication of this article. This work was supported by NIH grants NS 18400 and DK128315, and program project grant P01-HD32573 (PI: Gabriel Haddad). MLK was supported by grants institutional training grant T32-NS07455 (PI: Emile Boulpaep). WB was supported in part by a USAF studies and analysis grant 20-012.

Acknowledgments

The authors are very thankful to Annette Kolar for her input with the neurons culture and to Duncan Wong for computer and technical assistance during the project. We thank Michelle L. Kelly for her valuable input during early phases of the project. W.F.B gratefully acknowledges the support of the Myers/Scarpa endowed chair.

Conflict of interest

The authors declare that the research was conducted in the absence of any commercial or financial relationships that could be construed as a potential conflict of interest.

Publisher's note

References

Aronson, P. S., Nee, J., and Suhm, M. A. (1982). Modifier role of internal H^+ in activating the Na^+-H^+ exchanger in renal microvillus membrane vesicles. *Nature* 299, 161–163. doi:10.1038/299161a0

Baxter, K. A., and Church, J. (1996). Characterization of acid extrusion mechanisms in cultured fetal rat hippocampal neurones. *J. Physiol. (Lond.)* 493 (Pt 2), 457–470. doi:10.1113/jphysiol.1996.sp021396

Bevensee, M. O., Bashi, E., and Boron, W. F. (1999). Effect of trace levels of nigericin on intracellular pH and acid-base transport in rat renal mesangial cells. *J. Membr. Biol.* 169, 131–139. doi:10.1007/s002329900525

Bevensee, M. O., and Boron, W. F. (2013). "Control of intracellular pH," in *Seldin and giebisch's the kidney: physiology and pathophysiology* (Academic Press), 1773–1835.

Bevensee, M. O., Cummins, T. R., Haddad, G. G., Boron, W. F., and Boyarsky, G. (1996). pH regulation in single CA1 neurons acutely isolated from the hippocampi of immature and mature rats. *J. Physiol. (Lond)* 494, 315–328. doi:10.1113/jphysiol.1996.sp021494

Bevensee, M. O., Schwiening, C. J., and Boron, W. F. (1995). Use of BCECF and propidium iodide to assess membrane integrity of acutely isolated CA1 neurons from rat hippocampus. *J. Neurosci. Meth* 58, 61–75. doi:10.1016/0165-0270(94)00159-e

Boedtkjer, E., Hansen, K. B., Boedtkjer, D. M., Aalkjaer, C., and Boron, W. F. (2016). Extracellular HCO_3^- is sensed by mouse cerebral arteries: regulation of tone by receptor protein tyrosine phosphatase γ. *J. Cereb. Blood Flow. Metab.* 36, 965–980. doi:10.1177/0271678X15610787

Boron, W. F. (1985). Intracellular pH-regulating mechanism of the squid axon. Relation between the external Na^+ and HCO_3^- dependences. *J. Gen. Physiol.* 85, 325–345. doi:10.1085/jgp.85.3.325

Boron, W. F. (2004). Regulation of intracellular pH. *Adv. Physiol. Educ.* 28, 160–179. doi:10.1152/advan.00045.2004

Boron, W. F., and Boulpaep, E. L. (1983). Intracellular pH regulation in the renal proximal tubule of the salamander. Basolateral HCO_3^- transport. *J. Gen. Physiol.* 81, 53–94. doi:10.1085/jgp.81.1.53

Boron, W. F., and De Weer, P. (1976). Intracellular pH transients in squid giant axons caused by CO2, NH3, and metabolic inhibitors. *J. Gen. Physiol.* 67, 91–112. doi:10.1085/jgp.67.1.91

Boron, W. F., and Knakal, R. C. (1989). Intracellular pH-regulating mechanism of the squid axon. Interaction between DNDS and extracellular Na^+ and HCO_3^-. *J. Gen. Physiol.* 93, 123–150. doi:10.1085/jgp.93.1.123

Boron, W. F., and Knakal, R. C. (1992). Na^+-dependent Cl^--HCO_3^- exchange in the squid axon. Dependence on extracellular pH. *J. Gen. Physiol.* 99, 817–837. doi:10.1085/jgp.99.5.817

Boron, W. F., and Russell, J. M. (1983). Stoichiometry and ion dependencies of the intracellular-pH-regulating mechanism in squid giant axons. *J. Gen. Physiol.* 81, 373–399. doi:10.1085/jgp.81.3.373

Bouyer, P., Bradley, S. R., Zhao, J., Wang, W., Richerson, G. B., and Boron, W. F. (2004). Effect of extracellular acid-base disturbances on the intracellular pH of neurones cultured from rat medullary raphe or hippocampus. *J. Physiol. (Lond.)* 559, 85–101. doi:10.1113/jphysiol.2004.067793

Bouyer, P., Zhou, Y., and Boron, W. F. (2003). An increase in intracellular calcium concentration that is induced by basolateral CO_2 in rabbit renal proximal tubule. *Am. J. Physiol. Ren. Physiol.* 285, F674–F687. doi:10.1152/ajprenal.00107.2003

Bouyer, P. G., Taki, S., Moss, F., and Boron, W. (2024). Hypothesis and Theory: effects of extracellular metabolic acidosis on the homeostasis of intracellular pH in hippocampal neurons. *Front. Physiology* 15. doi:10.3389/fphys.2024.1406448

Boyarsky, G., Ganz, M. B., Sterzel, R. B., and Boron, W. F. (1988). pH regulation in single glomerular mesangial cells. I. Acid extrusion in absence and presence of HCO_3^-. *Am. J. Physiol. Cell Physiol.* 255, C844–C856. doi:10.1152/ajpcell.1988.255.6.C844

Brett, C. L., Kelly, T., Sheldon, C., and Church, J. (2002). Regulation of Cl^-/HCO_3^- exchangers by cAMP-dependent protein kinase in adult rat hippocampal CA1 neurons. *J. Physiol. (Lond.)* 545, 837–853. doi:10.1113/jphysiol.2002.027235

Brewer, G. J., Torricelli, J. R., Evege, E. K., and Price, P. J. (1993). Optimized survival of hippocampal neurons in B27-supplemented Neurobasal, a new serum-free medium combination. *J. Neurosci. Res.* 35, 567–576. doi:10.1002/jnr.490350513

Chen, L.-M., Kelly, M. L., Rojas, J. D., Parker, M. D., Gill, H. S., Davis, B. A., et al. (2008). Use of a new polyclonal antibody to study the distribution and glycosylation of the sodium-coupled bicarbonate transporter NCBE in rodent brain. *Neuroscience* 151, 374–385. doi:10.1016/j.neuroscience.2007.10.015

Chen, Y., Cann, M. J., Litvin, T. N., Iourgenko, V., Sinclair, M. L., Levin, L. R., et al. (2000). Soluble adenylyl cyclase as an evolutionarily conserved bicarbonate sensor. *Science* 289, 625–628. doi:10.1126/science.289.5479.625

Chesler, M. (2003). Regulation and modulation of pH in the brain. *Physiol. Rev.* 83, 1183–1221. doi:10.1152/physrev.00010.2003

Church, J., Baxter, K. A., and McLarnon, J. G. (1998). pH modulation of Ca^{2+} responses and a Ca^{2+}-dependent K^+ channel in cultured rat hippocampal neurones. *J. Physiol. (Lond.)* 511 (Pt 1), 119–132. doi:10.1111/j.1469-7793.1998.119bi.x

Cooper, D. S., Saxena, N. C., Yang, H. S., Lee, H. J., Moring, A. G., Lee, A., et al. (2005). Molecular and functional characterization of the electroneutral Na/HCO3 cotransporter NBCn1 in rat hippocampal neurons. *J. Biol. Chem.* 280, 17823–17830. doi:10.1074/jbc.M408646200

Cooper, D. S., Yang, H. S., He, P., Kim, E., Rajbhandari, I., Yun, C. C., et al. (2009). Sodium/bicarbonate cotransporter NBCn1/slc4a7 increases cytotoxicity in magnesium depletion in primary cultures of hippocampal neurons. *Eur. J. Neurosci.* 29, 437–446. doi:10.1111/j.1460-9568.2008.06611.x

Donowitz, M., Ming Tse, C., and Fuster, D. (2013). SLC9/NHE gene family, a plasma membrane and organellar family of Na^+/H^+ exchangers. *Mol. Asp. Med.* 34, 236–251. doi:10.1016/j.mam.2012.05.001

Eiden, L. E., Schäfer, M. K.-H., Weihe, E., and Schütz, B. (2004). The vesicular amine transporter family (SLC18): amine/proton antiporters required for vesicular accumulation and regulated exocytotic secretion of monoamines and acetylcholine. *Pflugers Arch.* 447, 636–640. doi:10.1007/s00424-003-1100-5

Ellis, D., and Thomas, R. C. (1976). Direct measurement of the intracellular pH of mammalian cardiac muscle. *J. Physiol. (Lond.)* 262, 755–771. doi:10.1113/jphysiol.1976.sp011619

Filosa, J. A., Dean, J. B., and Putnam, R. W. (2002). Role of intracellular and extracellular pH in the chemosensitive response of rat locus coeruleus neurones. *J. Physiol. (Lond.)* 541, 493–509. doi:10.1113/jphysiol.2001.014142

Gennari, F. J., and Weise, W. J. (2008). Acid-base disturbances in gastrointestinal disease. *Clin. J. Am. Soc. Nephrol.* 3, 1861–1868. doi:10.2215/CJN.02450508

Gurnett, C. A., Veile, R., Zempel, J., Blackburn, L., Lovett, M., and Bowcock, A. (2008). Disruption of sodium bicarbonate transporter *SLC4A10* in a patient with complex partial epilepsy and mental retardation. *Arch. Neurol.* 65, 550–553. doi:10.1001/archneur.65.4.550

Hentschke, M., Wiemann, M., Hentschke, S., Kurth, I., Hermans-Borgmeyer, I., Seidenbecher, T., et al. (2006). Mice with a targeted disruption of the Cl^-/HCO_3^- exchanger AE3 display a reduced seizure threshold. *Mol. Cell. Biol.* 26, 182–191. doi:10.1128/MCB.26.1.182-191.2006

Holzer, P. (2009). Acid-sensitive ion channels and receptors. *Handb. Exp. Pharmacol.*, 283–332. doi:10.1007/978-3-540-79090-7_9

Ishii, S., Kihara, Y., and Shimizu, T. (2005). Identification of T cell death-associated gene 8 (TDAG8) as a novel acid sensing G-protein-coupled receptor. *J. Biol. Chem.* 280, 9083–9087. doi:10.1074/jbc.M407832200

Jones, W. D., Cayirlioglu, P., Kadow, I. G., and Vosshall, L. B. (2007). Two chemosensory receptors together mediate carbon dioxide detection in Drosophila. *Nature* 445, 86–90. doi:10.1038/nature05466

Kanai, Y., Nussberger, S., Romero, M. F., Boron, W. F., Hebert, S. C., and Hediger, M. A. (1995). Electrogenic properties of the epithelial and neuronal high affinity glutamate transporter. *J. Biol. Chem.* 270, 16561–16568. doi:10.1074/jbc.270.28.16561

Keyes, S. R., and Rudnick, G. (1982). Coupling of transmembrane proton gradients to platelet serotonin transport. *J. Biol. Chem.* 257, 1172–1176. doi:10.1016/s0021-9258(19)68170-6

Kopito, R. R., Lee, B. S., Simmons, D. M., Lindsey, A. E., Morgans, C. W., and Schneider, K. (1989). Regulation of intracellular pH by a neuronal homolog of the erythrocyte anion exchanger. *Cell* 59, 927–937. doi:10.1016/0092-8674(89)90615-6

Lee, S.-K., Occhipinti, R., Moss, F. J., Parker, M. D., Grichtchenko, I. I., and Boron, W. F. (2023). Distinguishing among HCO_3^-, $CO_3^{=}$, and H^+ as substrates of proteins that appear to be "bicarbonate" transporters. *J. Am. Soc. Nephrol.* 34, 40–54. doi:10.1681/ASN.2022030289

Lesage, F. (2003). Pharmacology of neuronal background potassium channels. *Neuropharmacology* 44, 1–7. doi:10.1016/s0028-3908(02)00339-8

Li, S., Sato, S., Yang, X., Preisig, P. A., and Alpern, R. J. (2004). Pyk2 activation is integral to acid stimulation of sodium/hydrogen exchanger 3. *J. Clin. Invest.* 114, 1782–1789. doi:10.1172/JCI18046

Lim, S. (2007). Metabolic acidosis. *Acta Med. Indones.* 39, 145–150.

Ludwig, M.-G., Vanek, M., Guerini, D., Gasser, J. A., Jones, C. E., Junker, U., et al. (2003). Proton-sensing G-protein-coupled receptors. *Nature* 425, 93–98. doi:10.1038/nature01905

Meech, R. W., and Thomas, R. C. (1987). Voltage-dependent intracellular pH in *Helix aspersa* neurones. *J. Physiol. (Lond.)* 390, 433–452. doi:10.1113/jphysiol.1987.sp016710

Mohebbi, N., Benabbas, C., Vidal, S., Daryadel, A., Bourgeois, S., Velic, A., et al. (2012). The proton-activated G protein coupled receptor OGR1 acutely regulates the activity of epithelial proton transport proteins. *Cell. Physiol. biochem.* 29, 313–324. doi:10.1159/000338486

Montell, C. (2001). Physiology, phylogeny, and functions of the TRP superfamily of cation channels. *Sci. STKE* 2001, re1. doi:10.1126/stke.2001.90.re1

Parker, M. D., and Boron, W. F. (2013). The divergence, actions, roles, and relatives of sodium-coupled bicarbonate transporters. *Physiol. Rev.* 93, 803–959. doi:10.1152/physrev.00023.2012

Parker, M. D., Musa-Aziz, R., Rojas, J. D., Choi, I., Daly, C. M., and Boron, W. F. (2008). Characterization of human SLC4A10 as an electroneutral Na^+/HCO_3^- cotransporter (NBCn2) with Cl^- self-exchange activity. *J. Biol. Chem.* 283, 12777–12788. doi:10.1074/jbc.M707829200

Raley-Susman, K. M., Cragoe, E. J., Jr, Sapolsky, R. M., and Kopito, R. R. (1991). Regulation of intracellular pH in cultured hippocampal neurons by an amiloride-insensitive Na^+/H^+ exchanger. *J. Biol. Chem.* 266, 2739–2745. doi:10.1016/s0021-9258(18)49907-3

Raley-Susman, K. M., Sapolsky, R. M., and Kopito, R. R. (1993). Cl^-/HCO_3^- exchange function differs in adult and fetal rat hippocampal neurons. *Brain Res.* 614, 308–314. doi:10.1016/0006-8993(93)91049-x

Raphael, K. L. (2018). Metabolic acidosis and subclinical metabolic acidosis in CKD. *J. Am. Soc. Nephrol.* 29, 376–382. doi:10.1681/ASN.2017040422

Raphael, K. L., Murphy, R. A., Shlipak, M. G., Satterfield, S., Huston, H. K., Sebastian, A., et al. (2016). Bicarbonate concentration, acid-base status, and mortality in the health, aging, and body composition study. *Clin. J. Am. Soc. Nephrol.* 11, 308–316. doi:10.2215/CJN.06200615

Richmond, P. H., and Vaughan-Jones, R. D. (1997). Assessment of evidence for K^+-H^+ exchange in isolated type-1 cells of neonatal rat carotid body. *Pflugers Arch.* 434, 429–437. doi:10.1007/s004240050417

Romero, M. F., Chen, A.-P., Parker, M. D., and Boron, W. F. (2013). The SLC4 family of bicarbonate (HCO_3^-) transporters. *Mol. Asp. Med.* 34, 159–182. doi:10.1016/j.mam.2012.10.008

Roos, A., and Boron, W. F. (1981). Intracellular pH. *Physiol. Rev.* 61, 296–434. doi:10.1152/physrev.1981.61.2.296

Ruffin, V. A., Salameh, A. I., Boron, W. F., and Parker, M. D. (2014). Intracellular pH regulation by acid-base transporters in mammalian neurons. *Front. Physiol.* 5, 43. doi:10.3389/fphys.2014.00043

Russell, J. M., and Boron, W. F. (1976). Role of choloride transport in regulation of intracellular pH. *Nature* 264, 73–74. doi:10.1038/264073a0

Salameh, A. I., Hübner, C. A., and Boron, W. F. (2017). Role of Cl^--HCO_3^- exchanger AE3 in intracellular pH homeostasis in cultured murine hippocampal neurons, and in crosstalk to adjacent astrocytes. *J. Physiol. (Lond.)* 595, 93–124. doi:10.1113/JP272470

Salameh, A. I., Ruffin, V. A., and Boron, W. F. (2014). Effects of metabolic acidosis on intracellular pH responses in multiple cell types. *Am. J. Physiol. Regul. Integr. Comp. Physiol.* 307, R1413–R1427. doi:10.1152/ajpregu.00154.2014

Schulz, S., Wedel, B. J., Matthews, A., and Garbers, D. L. (1998). The cloning and expression of a new guanylyl cyclase orphan receptor. *J. Biol. Chem.* 273, 1032–1037. doi:10.1074/jbc.273.2.1032

Schwiening, C. J., and Boron, W. F. (1994). Regulation of intracellular pH in pyramidal neurones from the rat hippocampus by Na^+-dependent Cl^--HCO_3^- exchange. *J. Physiol. (Lond)* 475, 59–67. doi:10.1113/jphysiol.1994.sp020049

Smith, G. A., Brett, C. L., and Church, J. (1998). Effects of noradrenaline on intracellular pH in acutely dissociated adult rat hippocampal CA1 neurones. *J. Physiol. (Lond.)* 512 (Pt 2), 487–505. doi:10.1111/j.1469-7793.1998.487be.x

Sun, L., Wang, H., Hu, J., Han, J., Matsunami, H., and Luo, M. (2009). Guanylyl cyclase-D in the olfactory CO_2 neurons is activated by bicarbonate. *Proc. Natl. Acad. Sci. U.S.A.* 106, 2041–2046. doi:10.1073/pnas.0812220106

Sun, X., Yang, L. V., Tiegs, B. C., Arend, L. J., McGraw, D. W., Penn, R. B., et al. (2010). Deletion of the pH sensor GPR4 decreases renal acid excretion. *J. Am. Soc. Nephrol.* 21, 1745–1755. doi:10.1681/ASN.2009050477

Svichar, N., Waheed, A., Sly, W. S., Hennings, J. C., Hübner, C. A., and Chesler, M. (2009). Carbonic anhydrases CA4 and CA14 both enhance AE3-mediated Cl^--HCO_3^- exchange in hippocampal neurons. *J. Neurosci.* 29, 3252–3258. doi:10.1523/JNEUROSCI.0036-09.2009

Taki, S., Boron, W. F., and Moss, F. J. (2024). Novel RPTPγ and RPTPζ splice variants from mixed neuron-astrocyte hippocampal cultures as well as from the hippocampi of newborn and adult mice. *Front. Physiol.* 15, 1406448. doi:10.3389/fphys.2024.1406448

Tang, C. M., Dichter, M., and Morad, M. (1990). Modulation of the N-methyl-D-aspartate channel by extracellular H^+. *Proc. Natl. Acad. Sci. U.S.A.* 87, 6445–6449. doi:10.1073/pnas.87.16.6445

Thomas, J. A., Buchsbaum, R. N., Zimniak, A., and Racker, E. (1979). Intracellular pH measurements in Ehrlich ascites tumor cells utilizing spectroscopic probes generated *in situ*. *Biochemistry* 18, 2210–2218. doi:10.1021/bi00578a012

Thomas, R. C. (1977). The role of bicarbonate, chloride and sodium ions in the regulation of intracellular pH in snail neurones. *J. Physiol. (Lond.)* 273, 317–338. doi:10.1113/jphysiol.1977.sp012096

Thornell, I. M., Michenkova, M., Taki, S., Bevensee, M. O., and Boron, W. F. (2025). "Intracellular pH homeostasis," in *Seldin and giebisch's the kidney: physiology and pathophysiology*. Editors R. J. Alpern, M. J. Caplan, O. W. Moe, and S. E. Quaggin (London: Elsevier/Academic Press). Available at: https://www.barnesandnoble.com/w/seldin-and-giebischs-the-kidney-robert-j-alpern/1138252983 (Accessed August 29, 2023).

Tolkovsky, A. M., and Richards, C. D. (1987). Na^+/H^+ exchange is the major mechanism of pH regulation in cultured sympathetic neurons: measurements in single cell bodies and neurites using a fluorescent pH indicator. *Neuroscience* 22, 1093–1102. doi:10.1016/0306-4522(87)92984-8

Tomura, H., Mogi, C., Sato, K., and Okajima, F. (2005). Proton-sensing and lysolipid-sensitive G-protein-coupled receptors: a novel type of multi-functional receptors. *Cell. Signal.* 17, 1466–1476. doi:10.1016/j.cellsig.2005.06.002

Tresguerres, M., Buck, J., and Levin, L. R. (2010). Physiological carbon dioxide, bicarbonate, and pH sensing. *Pflugers Arch.* 460, 953–964. doi:10.1007/s00424-010-0865-6

Vaughan-Jones, R. D. (1986). An investigation of chloride-bicarbonate exchange in the sheep cardiac Purkinje fibre. *J. Physiol. (Lond.)* 379, 377–406. doi:10.1113/jphysiol.1986.sp016259

Vittinghoff, E., Shiboski, S. C., Glidden, D. V., and McCulloch, C. E. (2005). *Regression methods in biostatistics Linear, logistic, survival, and repeated measures models*. Springer Science and Business Media, Inc.

Wang, W., Bradley, S. R., and Richerson, G. B. (2002). Quantification of the response of rat medullary raphe neurones to independent changes in pH_o and P_{CO2}. *J. Physiol. (Lond.)* 540, 951–970. doi:10.1113/jphysiol.2001.013443

Yao, H., Ma, E., Gu, X. Q., and Haddad, G. G. (1999). Intracellular pH regulation of CA1 neurons in Na(+)/H(+) isoform 1 mutant mice. *J. Clin. Invest.* 104, 637–645. doi:10.1172/JCI6785

Zhao, J., Hogan, E. M., Bevensee, M. O., and Boron, W. F. (1995). Out-of-equilibrium CO_2/HCO_3^- solutions and their use in characterizing a new K^+/HCO_3^- cotransporter. *Nature* 374, 636–639. doi:10.1038/374636a0

Zhao, J., Zhou, Y., and Boron, W. F. (2003). Effect of isolated removal of either basolateral HCO_3^- or basolateral CO_2 on HCO_3^- reabsorption by rabbit S2 proximal tubule. *Am. J. Physiol. Ren. Physiol.* 285, F359–F369. doi:10.1152/ajprenal.00013.2003

Zhou, Y., Skelton, L. A., Xu, L., Chandler, M. P., Berthiaume, J. M., and Boron, W. F. (2016). Role of receptor protein tyrosine phosphatase γ in sensing extracellular CO_2 and HCO_3^-. *J. Am. Soc. Nephrol.* 27, 2616–2621. doi:10.1681/ASN.2015040439

Zhou, Y., Zhao, J., Bouyer, P., and Boron, W. F. (2005). Evidence from renal proximal tubules that HCO_3^- and solute reabsorption are acutely regulated not by pH but by basolateral HCO_3^- and CO_2. *Proc. Natl. Acad. Sci. U.S.A.* 102, 3875–3880. doi:10.1073/pnas.0500423102